Geophysical Journal International

Geophys. J. Int. (2015) **201,** 1038–1059 doi: 10.1093/gji/ggv060
GJI Geodynamics and tectonics

Imaging the mantle lithosphere of the Precambrian Grenville Province: large-scale electrical resistivity structures

Ademola Q. Adetunji,[1] Ian J. Ferguson[1] and Alan G. Jones[2]

[1]*Department of Geological Sciences, University of Manitoba, Winnipeg, Canada. E-mail: Ademola.Adetunji@umanitoba.ca*
[2]*Dublin Institute for Advanced Studies, Dublin, Ireland*

Accepted 2015 February 5. Received 2015 February 4; in original form 2014 October 10

SUMMARY

The resistivity structure of the lithospheric mantle beneath the Proterozoic Grenville Province in southern Ontario, Canada is investigated using 84 magnetotelluric (MT) sites divided into four profiles. Depth-based regional geoelectric dimensionality analyses of the MT responses indicate that the mantle lithosphere north of Lake Ontario can be subdivided into upper (45–150 km) and deeper (>200 km) lithospheric mantle layers with regional strike azimuths of N85°E (±5°) and N65°E (±5°), respectively. MT responses from the Grenville Front and the northwest part of the Central Gneiss Belt are compatible with the presence of 2-D resistivity structures but farther to the southeast, in the southeast part of the Central Gneiss Belt and Central Metasedimentary Belt, they suggest the presence of localized 3-D structures. 2-D inversion of distortion-free MT responses images a large scale very resistive (>20 000 Ω m) region that extends 300 km southeast of the Grenville Front and for at least 800 km along-strike in the lithospheric mantle beneath the Grenville Province. This feature is interpreted to be Superior Province lithosphere and the corresponding N85°E geoelectric strike to be associated with the fabric of the Superior Province. The base of the resistor reaches depths of 280 km on two of the three MT profiles north of Lake Ontario and this depth is interpreted to be the base of the lithosphere. A large region of enhanced conductivity in the lower lithosphere, spatially correlated with decreased seismic velocity, is bounded to the northwest by a subvertical resistivity anomaly located near the Kirkland Lake and Cobalt kimberlite fields. The enhanced conductivity in the lower lithosphere is attributed to refertilization by fluids associated with Cretaceous kimberlite magmatism and can be explained by water content in olivine of 50 wt ppm in background areas with higher values in a localized anomaly beneath the kimberlite fields. Farther to the southeast the resistivity models include a lithospheric conductor between 100 and 150 km depth beneath the Central Metasedimentary Belt. The enhanced conductivity is attributed to grain boundary graphite films, associated with the Cretaceous kimberlitic magmatic process, or to water and carbon, introduced into the mantle during the pre-Grenvillian tectonism.

Key words: Electrical properties; Magnetotellurics; Composition of the mantle; Cratons; North America.

1 INTRODUCTION

In this study we use the magnetotelluric (MT) method to image the electrical resistivity structure of the mantle lithosphere beneath the Grenville Province in southern Ontario, Canada (Fig. 1). Electromagnetic (EM) images of continental lithosphere help elucidate its formation, preservation and deformation (e.g. Jones 1999; Davis *et al.* 2003; Ferguson *et al.* 2012). Sources of enhanced conductivity in the mantle include graphite, water, partial melt, temperature and hydrogen (e.g. Karato 1990; Mibe *et al.* 1998; Jones 1999; Ducea & Park 2000; Hirth *et al.* 2000; Constable 2006; Korja 2007; Yoshino *et al.* 2008; Muller *et al.* 2009; Selway 2014). Because of the many possible sources, interpretation of enhanced lithospheric mantle conductivity must always consider local geological and physical conditions (Schwarz 1990; Korja 2007; Selway 2014).

Previous MT investigations in the study area have revealed resistive mantle lithosphere beneath the southeastern Superior craton and Grenville Front (Kellett *et al.* 1992, 1994; Mareschal *et al.* 1995). In these studies, the MT responses were also interpreted to indicate the presence of electrical anisotropy in the lithosphere (e.g. Kurtz *et al.* 1988; Kellett *et al.* 1992, 1994; Mareschal *et al.* 1995; Zhang *et al.* 1995; Ji *et al.* 1996; Sénéchal *et al.* 1996; Boerner *et al.* 2000; Frederiksen *et al.* 2006). More recently, Adetunji *et al.* (2014) used 2-D inversion to show that resistive mantle lithosphere occurs

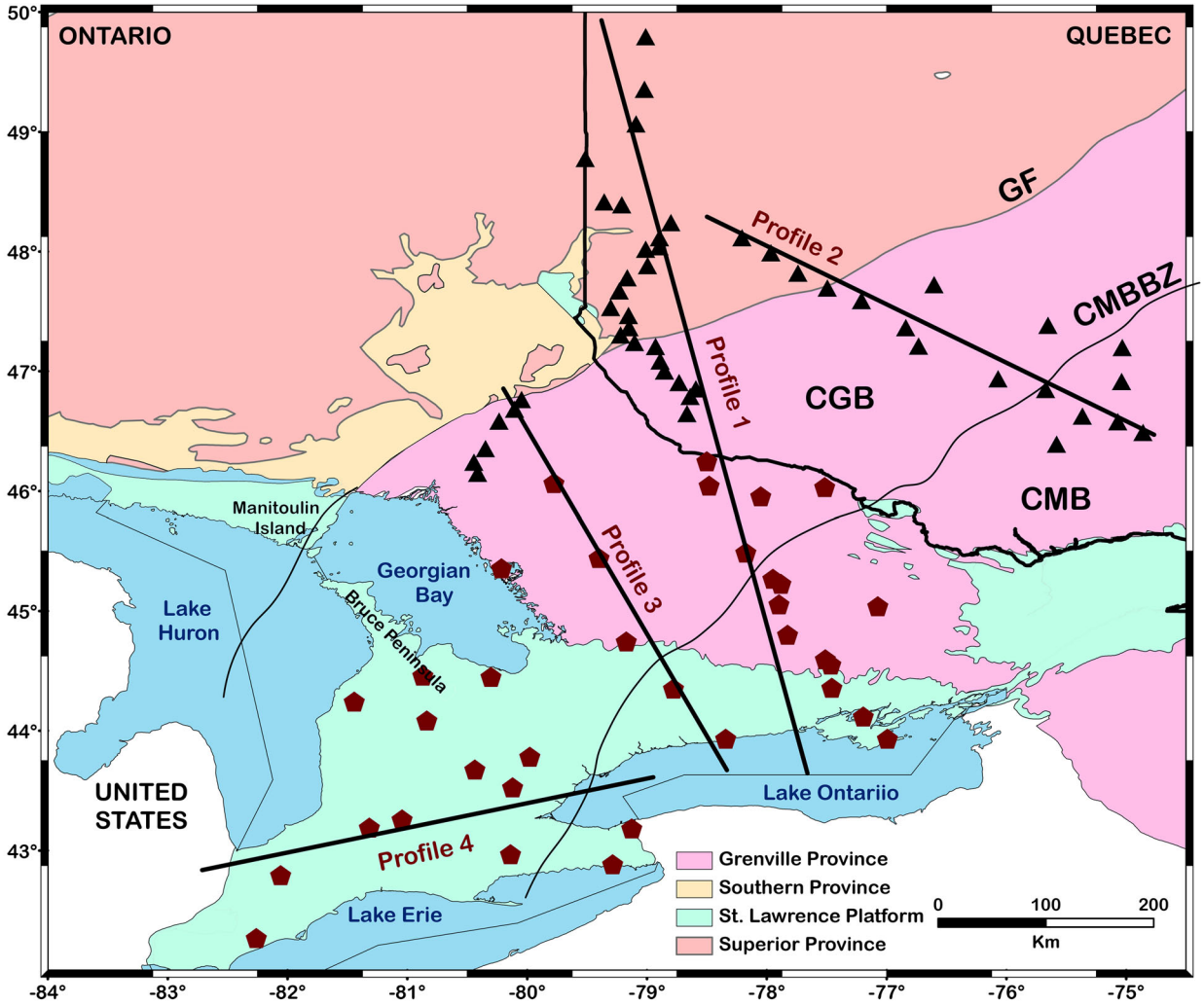

Figure 1. Map of the study area showing the locations of MT sites considered in this study. The black triangles indicate MT sites from the Lithoprobe-Abitibi Grenville transect and the wine-coloured diamonds indicate POLARIS MT sites. Profile 1 has been analysed by Adetunji *et al.* (2014). The tectonic elements include the Grenville Front (GF), Central Gneiss belt (CGB), Central Metasedimentary Belt (CMB) and Central Metasedimentary Belt Boundary Zone (CMBBZ).

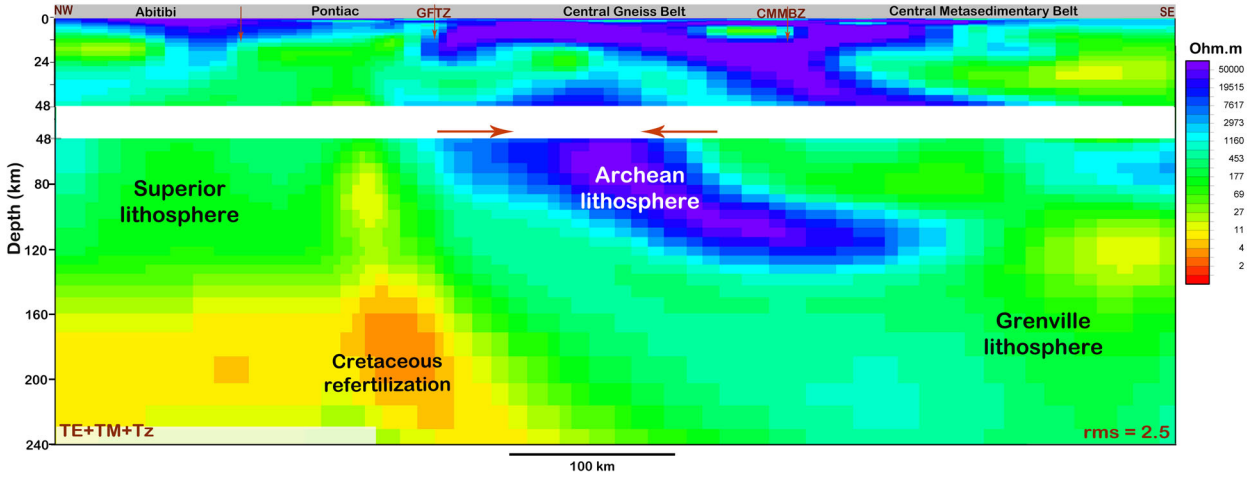

Figure 2. Crustal and lithospheric mantle resistivity model (V.E. = 1) determined by Adetunji *et al.* (2014) for Profile 1 (Fig. 1). The crustal model is based on a geoelectric strike of N45°E and the lithospheric model is based on a strike of N85°E. Labels show the interpretations of Adetunji *et al.* (2014) of lithospheric mantle resistivity structures. GFTZ, Grenville Front Tectonic Zone; CMBBZ, Central Metasedimentary Belt Boundary Zone. Arrows mark position of the resistive lithosphere in the uppermost mantle.

between 50 and 150 km depth in the northwestern Grenville Province and extends 300 km south of the Grenville Front (Fig. 2). They show that the observed MT responses can, in fact, be accurately modelled by isotropic 2-D models.

In other related studies Mareschal *et al.* (1991) analysed data from an MT profile crossing the Grenville Front on Manitoulin Island and the Bruce Peninsular. At this location, resolution of the underlying lithospheric resistivity structure is severely limited by the conductive Phanerozoic rocks at the surface, and the MT data are only able to place a broad lower limit on the underlying resistivity of 500 Ω m. Ogawa *et al.* (1996) and Wannamaker *et al.* (1996) present 2-D models from the southeastern United States that show the signature of the Grenville orogen. The Grenville suture is imaged as a conductive feature in the uppermost mantle.

In this work we use a larger MT data set than in earlier studies by Kellett *et al.* (1992, 1994) and Mareschal *et al.* (1995) along with modern tensor decomposition and isotropic 2-D inversions, to investigate the large-scale resistivity structure of the Grenville Province. A total of 84 broad-band MT sites distributed across the southern Ontario, are analysed (Fig. 1). These sites, collected in the LITHOPROBE Abitibi-Grenville transect (Boerner *et al.* 2000) and POLARIS (Portable Observatories for Lithospheric Analysis and Research Investigating Seismicity) southern Ontario array (Eaton *et al.* 2005), are subdivided into four profiles. Profiles 1–3 are located to the north of Lake Ontario and for most of their length cross exposed Precambrian rocks (Fig. 1). Profile 4 is located to west of Lake Ontario, between Lake Erie and Lake Huron on Phanerozoic rocks of the Michigan Basin (Fig. 1). Profiles 1 and 3 combine data from the LITHOPROBE and POLARIS projects; Profile 2 contains mainly LITHOPROBE sites whereas Profile 4 includes only POLARIS MT sites. The MT data from Profile 1 have been examined previously by Kellett *et al.* (1992, 1994), Zhang *et al.* (1995), Mareschal *et al.* (1995), Ji *et al.* (1996), Sénéchal *et al.* (1996) and Adetunji *et al.* (2014). Mareschal *et al.* (1995) and Boerner *et al.* (2000) examine anistropy in the MT response for sites in profiles 1-3 and Frederiksen *et al.* (2006) examine anisotropy in the MT response for all four profiles. This study presents the first modelling of responses from Profiles 2–4.

Specific components and objectives of this study are as follows:

(1) Determination of the geoelectric dimensionality and optimal regional strike, as a function of depth, for 2-D modelling and inversion of the MT data from each profile over a broad region of the Grenville Province. An expanded MT data set and modern depth-based dimensionality and strike determination will provide improved understanding of the resistivity structures present in the lithospheric mantle in the area.

(2) Definition of the spatial extent of the resistive lithosphere identified in the earlier MT studies (Mareschal *et al.* 1995; Adetunji *et al.* 2014): The inclusion of Profiles 2–4 will define the along-strike extent of this feature.

(3) Synthesis of the MT results with other geophysical and geological constraints to provide an updated interpretation of the geological cause and tectonic history of the resistive mantle lithosphere in the Grenville Province.

2 TECTONIC SETTING

The Grenville Province is part of the Middle to Late Mesoproterozoic Grenville (1.2–1.0 Ga) orogen, extending across North America from Mexico to Labrador (Hanmer 1988; Easton 1992; Rivers 1997; Carr *et al.* 2000; Rivers *et al.* 2012). It is composed of reworked polycyclic Archean, Palaeo- and Meso-Proterozoic rocks derived from Laurentia (proto-North American landmass) as well as monocyclic rocks accreted just prior to the Grenvillian orogeny (Hoffman 1989; Rivers *et al.* 1993, 2012; Carr *et al.* 2000). The Grenville Province is separated from older units such as the Superior and Southern provinces, the Killarney Magmatic Belt, the Eastern Granite-Rhyolite province and the Midcontinent Rift by the Grenville Front (GF; Williams *et al.* 1992).

In southern Ontario, the Grenville Province (Fig. 1) is bounded by the GF to the northwest, where it overlies the Southern and Superior provinces. It is subdivided into the Central Gneiss Belt (CGB) and the Central Metasedimentary Belt (CMB) (Wynne-Edwards 1972; Easton 1992). The tectonic contact between the CGB and CMB is a northeast–southwest trending set of ductile shear zones called the Central Metasedimentary Belt Boundary Zone (CMBBZ; Wynne-Edwards 1972; Easton 1992). The CGB represents part of the reworked margin of the pre-Grenvillian Laurentian craton (Easton 1992). The CMB represents a major Mesoproterozoic accretion of supracrustal rocks and was thrust northwestwardly over the CGB (Davidson 1991; Easton 1992; Davidson 1998). In the southwest part of the study area, the Proterozoic Grenville Province is interpreted to be bounded to the west by the Proterozoic Mazatzal Province (Whitmeyer & Karlstrom 2007). In this area the Precambrian basement is covered by the Michigan Basin so there is some uncertainty in this interpretation.

The youngest tectonic event associated with the study area is the Great Meteor hotspot (Crough 1981; Sleep 1990). This hotspot is interpreted to be responsible for the emplacement of the Cretaceous Monteregian–White Mountain–New England Seamounts Igneous Province (Crough 1981; Sleep 1990). It is also interpreted to be associated with the Mesozoic kimberlite magmatism in the Rapide des Quinze (Ji *et al.* 1996) and Kirkland Lake (Meyer *et al.* 1994; Ji *et al.* 1996) areas of the Pontiac subprovince (Griffin *et al.* 2004; Faure *et al.* 2011).

3 DIMENSIONALITY ANALYSIS

3.1 Method

The primary response derived from MT data is the complex-valued impedance tensor. Individual terms of the tensor may be examined in terms of the corresponding apparent resistivity and impedance phase, both of which give insight into underlying resistivity structure (Vozoff 1991; Chave & Jones 2012). Determination of the dimensionality of the subsurface resistivity structure is required in order to apply appropriate data inversion methods and can be accomplished by analysis of the MT tensor responses. The resistivity structure can be 1-D or horizontally layered, 2-D with a geoelectric strike along which the resistivity is invariant or it may have a more complex 3-D structure. An MT response may also be distorted galvanically by small-scale, near-surface, heterogeneities. In this case, the MT phase response is a more robust response than the apparent resistivity. Using tensor decomposition methods the true regional phase response can be recovered exactly from distorted responses whereas after the decomposition the apparent resistivity may still be affected by a period-independent static shift (Jones 1988, 2012).

In this study, dimensionality analysis is applied using Groom–Bailey (GB) tensor decomposition. This method determines the geoelectric strike simultaneously with parametrization of the galvanic distortion. In its original form (Groom & Bailey 1989, 1991), GB decomposition was applied to particular period bands in the responses at single sites and in the McNeice–Jones extension of

the GB method (GB–MJ) it was applied to particular period bands at multiple sites. However, because the penetration of MT signals depends on both the period of the signal and the local resistivity, for a study area with strong resistivity variations, this approach will mix dimensionality results from different depths. The GB–MJ method has now been modified to use depth ranges rather than period bands by incorporation of Niblett–Bostick depth transforms (e.g. Hamilton *et al.* 2006; Miensopust *et al.* 2011) and in this form it allows superior examination of the dimensionality and strike for a particular depth range. The Niblett–Bostick depth transform for Profile 1 is described in Adetunji *et al.* (2014). We apply the depth-dependent GB–MJ approach, as implemented in the STRIKE program of McNeice & Jones (2001), to examine the dimensionality of large-scale resistivity structures in the Grenville province and optimal strike directions for 2-D inversions.

Adetunji *et al.* (2014) showed that there is a significant change in the geoelectric strike azimuth for Profile 1 at a depth of about 200 km. Further analysis, using 50-km-thick depth bands, and phase tensor analysis (Caldwell *et al.* 2004) show that the change in azimuth occurs at ∼150 km depth (Adetunji 2014). This depth corresponds to the base of the large-scale resistive zone in the upper mantle on the profile (Fig. 2). In this study we therefore define GB dimensionality and strike azimuth for depth bands corresponding to the upper lithospheric mantle (45–150 km) and a deeper layer (>200 km). We refer to the lower layer as the 'deeper mantle layer' because the relative contribution in this depth range from the lower lithosphere and asthenosphere is not yet fully established. Results were also obtained for crustal depths but are not reported here.

The GB–MJ algorithm fits a regional MT response to a group of periods, or their equivalent depths, and sites by minimizing the total squared misfit between observed and predicted impedances (e.g. Hamilton *et al.* 2006; Muller *et al.* 2009; Miensopust *et al.* 2011). Positive attributes of the GB method are that it uses all of the information in the impedance tensor and that it accommodates errors in the MT data in an appropriate statistical manner. A negative attribute is the required assumption of a regional 2-D resistivity model, although the validity of that assumption is tested statistically by the method. The quality of the fit of the GB model to an observed data set provides a measure of the three-dimensionality of the regional structure. A large normalized rms misfit provides an indication that the data are unable to be explained by a 1-D or 2-D regional resistivity structure, or that the impedance errors have been improperly estimated and are too small. In this study, the GB–MJ misfits were calculated using the default impedance error floor of 3.5 per cent, which corresponds to a 7 per cent error for the apparent resistivity and 2° for phase. This floor is calculated based on the largest impedance value, and applied in an absolute manner to the other three. For these values, normalized rms misfits exceeding 2.0 are often regarded as indicative of significantly 3-D structures (Jones 2012).

3.2 Results

The data at almost all of the sites on Profiles 1–3 have Niblett–Bostick depth penetration to a depth of 150 km, beyond which there is penetration at fewer sites. For Profile 4, the conductive sedimentary basin rocks at the surface limit the penetration at most sites to less than 150 km. The results of the GB-MJ analysis show that the Grenville Province is characterized by dominantly 2-D MT responses. For most of the sites, the rms misfit of the 2-D regional model is less than 1.0. However, at isolated sites, particularly in the CMB values of up to 4.0 occur. The results also exhibit constancy of strike azimuths over spatial scales on the order of hundreds of kilometres providing a further indicator of two-dimensionality.

Primary observations that can be drawn from strike azimuths (Fig. 3) on Profiles 1–3 to the north of Lake Ontario are:

(1) Spatially consistent conductive directions are observed in the upper lithospheric mantle from the southern Superior craton to locations in the CGB that lie within approximately 100 km southeast of the Grenville Front. The southeast limit of this region is marked by the dashed line in Fig. 3. On Profiles 1 and 2 azimuths in this region are ∼N85°E (E15°N) whereas on Profile 3 they are N110°E (E20°S).

(2) In the southwestern CGB and CMB the conductive directions in the upper lithospheric mantle are more erratic, but the majority of sites have conductive directions parallel or perpendicular to a N45°E azimuth.

(3) Across the whole area, azimuths at deeper lithospheric mantle depths are mostly parallel or perpendicular to a ∼N45°E direction. For Profiles 1 and 2 the conductive direction is N45°E but for sites in the CGB on Profile 3 it is E45°S.

For Profile 4 strike azimuths are available only for the upper lithospheric depth range. The directions of strike azimuths for this depth range are reasonably consistent across the profile. At most sites there is an approximately east–west or north–south azimuth. The bimodal response is explained by the inherent 90° ambiguity in all impedance strike determination methods.

4 DETERMINATION OF 2-D INVERSION AZIMUTHS

The tensor decomposition results presented above provide justification for the application of 2-D modelling to the data from individual profiles. The upper lithospheric mantle and deeper mantle conductive directions show reasonable azimuthal consistency over each of the profiles (Fig. 3), particularly Profiles 1 and 2. Three-dimensionality indicators including the GB rms misfits, strong spatial variations in the strike azimuth, and phase tensor skews (Adetunji 2014; Adetunji *et al.* 2015) are relatively low over the northern half of each profile. The long-period induction arrow response for the area (Adetunji 2014; Adetunji *et al.* 2015) includes arrows that are dominantly oblique to the strike azimuths and provides further support for a 2-D modelling approach. In this section we use GB decomposition methods to establish the optimal geoelectric strike for 2-D modelling the data from each profile.

4.1 Methodology

To determine a regional geoelectric strike for the 2-D modelling of each of the profiles, four methods are used to assess the strike and its uncertainty. Each of the methods makes use of the GB misfit for a single depth estimate at a single site. The squared GB misfit for site j for each depth estimate k is defined in terms of reparametrized impedance terms $\alpha_0 = Z_{xx} + Z_{yy}$, $\alpha_1 = Z_{xy} + Z_{yx}$, $\alpha_2 = Z_{yx} - Z_{xy}$ and $\alpha_3 = Z_{xx} - Z_{yy}$ as:

$$e^2_{jk} = \sum_{i=0}^{3} \left[\frac{\left(\mathrm{Re}\,\alpha^{\mathrm{obs}}_{ijk} - \mathrm{Re}\,\alpha^{\mathrm{model}}_{ijk}\right)}{\sigma_{\alpha_{ijk}}} \right]^2 + \sum_{i=0}^{3} \left[\frac{\left(\mathrm{Im}\,\alpha^{\mathrm{obs}}_{ijk} - \mathrm{Im}\,\alpha^{\mathrm{model}}_{ijk}\right)}{\sigma_{\alpha_{ijk}}} \right]^2, \quad (1)$$

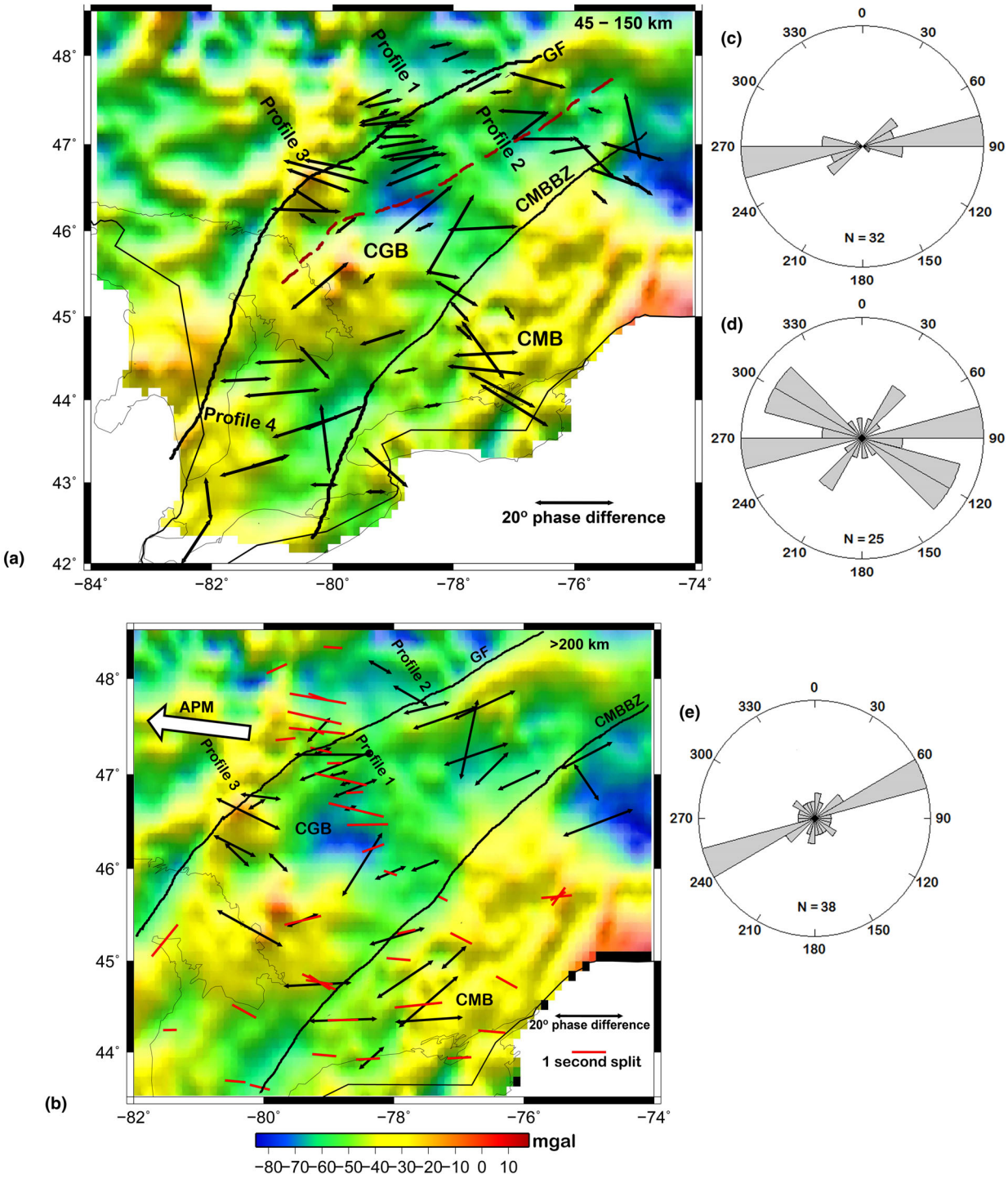

Figure 3. GB strike azimuths for (a) the upper lithospheric depth range (45–150 km) and (b) underlying mantle depths (>200 km). The black arrows show the azimuth of the GB regional impedance with the highest phase. The length of the arrow is proportional to the average phase difference, between the maximum and minimum phase values over the depth band. The dashed red line on the upper panel shows the southeast limit of the region with consistent azimuth in the upper lithospheric mantle. The red lines show the SKS fast direction defined by Sénéchal *et al.* (1996), Eaton *et al.* (2004), Rondenay *et al.* (2000), Evans *et al.* (2006) and Frederiksen *et al.* (2006, 2007) scaled by the time split. The plots are superimposed on the regional Bouguer gravity anomaly map (data obtained from Geological Survey of Canada). The white arrow, APM, shows the GPS-based absolute plate motion direction defined by Larson *et al.* (1997). (c) Rose diagram of the strike azimuth for sites northwest of the dashed line on Profiles 1–3 for 45–150 km depth range (d) Rose diagram of the strike azimuth for sites southeast of the dashed line on Profiles 1–3 for 45–150 km depth range. (e) Rose diagram of the strike azimuth of the deeper mantle layer.

where the model response depend on the GB distortion parameters and the regional strike θ_r for the depth band under consideration and σ_α is the estimated standard deviation for each datum (Groom & Bailey 1989; McNeice & Jones 2001).

A common experience in GB decomposition of MT data from sites in Precambrian crystalline terranes is that the minimization provides statistically reasonable levels of misfit for the data from most sites, but very poor results for the data at a small number of the

sites. The observations suggest that the 'geological noise' in the GB fit (e.g. local departures of the data from the underlying assumption of a 1-D or 2-D structure) is distributed unevenly between sites. The higher levels of noise at some sites may be due to a strong local 3-D inductive response or to other effects. A common approach in this situation is to simply remove those sites and repeat the GB analysis. Here, we examine the possibility of using more robust estimate of the misfit.

The suite of methods we used is as follows:

Method 1: The first estimate is the normal multi-site regional strike provided by GB–MJ method implemented in the STRIKE program. This estimate is for the regional strike that minimizes the summed squared misfit for the band of depths and for a group of sites:

$$E_1 = \frac{1}{MN}\sum_{j=1}^{M}\sum_{k-1}^{N} e_{jk}^2 \tag{2}$$

Method 2: The second method involves calculating and plotting the total squared error $e_j^2(\theta_r)$ for the depth band for individual sites at specified values of the regional strike (e.g. Schmoldt 2011). This method permits examination of how different sites contribute to the constraint of the regional strike through inspection of the rms error distribution along the profile.

Method 3: The third method is based on examining a sum of the absolute value of the error for a range of specified values of the regional strike:

$$E_2(\theta_r) = \frac{1}{MN}\sum_{j=1}^{M}\sum_{k=1}^{N} |e_{jk}|, \tag{3}$$

The use of an L_1 norm means that this measure will be less sensitive than the GB–MJ measure E_1 to individual sites with very large misfits. Plots of E_2 versus θ_r (e.g. Pous *et al.* 1997) can be used to obtain a visual estimate of the uncertainty in the strike azimuth; broad minima indicate poorly resolved strikes whereas narrow minima indicate tightly resolved azimuths.

Method 4: In the final method an additional allowance is made for outliers in the noise at different sites by using the median rather than the mean of the depth-band misfits:

$$E_3(\theta_r) = \text{median}\left[\frac{1}{N}\sum_{k=1}^{N} |e_{jk}|\right] \tag{4}$$

For all analyses we used depth bands corresponding to the upper lithospheric mantle (45–150 km) and deeper mantle layer (>200 km). The analyses used the default impedance error floor of 3.5 per cent. Methods 2–4 were implemented using single-site decomposition and regional strike angles constrained from 0° to 90° with 1° increments. We extracted the individual misfit values for each site and depth range from the output files of the McNeice & Jones (2001) STRIKE program.

During the analyses it was found that, despite being more robust to sites with higher noise levels, methods 3 and 4 usually failed to produce reasonable results if data from such sites were included. For example, erratic jumps occurred in error versus strike angle when these sites were used. These effects are attributed to the complexity of the GB misfit in the presence of noisy data. Despite this limitation, the availability of the full suite of strike results enhanced the strike determination process. We used methods 2, 3 and 4 to choose sites to exclude from the final analyses, method 2 to determine which sites controlled the final strike, and methods 3 and 4 to estimate the confidence in the strike results. Figs 4–6 show results from these methods and the regional strikes determined from all methods are listed in Table 1. Adetunji *et al.* (2014) describe the GB shear and twist values determined for sites along Profile 1.

4.2 Common strike azimuth for the upper lithospheric mantle

4.2.1 *Profile 1*

As shown in Fig. 5, sites that are more sensitive to the strike direction on Profile 1 come from those sites northwest of the Grenville Front and in the northwestern CGB. These sites all exhibit lowest misfit for strike directions between about N75°E and N90°E. The azimuth is less well defined in the southeastern CGB, but the data at most sites are compatible with a similar result to that observed farther north. The response at sites in the CMB is far more erratic with several sites having large misfits at all regional strike azimuths (PSO003, PSO013 and PSO042). At sites where the azimuth is better defined (e.g. PSO014, PSO040, PSO041 and PSO001), the minimum misfit occurs for a southwest–northeast strike with an azimuth between about N45°E and N65°E.

After excluding sites with high rms misfit (PSO001, PSO003, PSO009, PSO013, PSO042 and PSO039) from the analysis, the MJ–GB multisite multifrequency analysis yields an optimal direction of N85°E for the profile. The graphs of E_2 and E_3 versus strike angle obtained after exclusion of the same sites, exhibit broad minima between N70°E and N90°E (Fig. 4). Using these graphs we determine an overall strike angle for the profile of N80°E ±10°. The GB–MJ result lies well inside this range. Taken together, the results for Profile 1 indicate that N85°E is the appropriate strike angle for 2-D inversion. However, the part of the inversion model corresponding to the CMB, where the true strike angle is closer to N55°E, will need to be interpreted cautiously.

4.2.2 *Profile 2*

With the exception of sites GRE006 and GRE028 the misfit is relatively low for all sites and all azimuths on Profile 2 (Fig. 5). The misfit values for this depth range are lower than on the other profiles. Schmoldt (2011) suggests that responses where rms misfits are low in most directions indicate locally 1-D subsurface resistivity structure. However, this observation can also occur in 2-D structures for which the TE and TM phase curves cross or take on similar values at the periods corresponding to the depth range under consideration.

The geoelectric strike direction for Profile 2 determined by MJ–GB (N85°E) agrees well the azimuth determined by the minimum of E_2 (N85°E ±4°) and E_3 (N80°E ±6°). Misfit curves for Methods 3 and 4 show that the optimal strike direction for Profile 2 is defined more accurately than for Profile 1. The results for Profile 2 indicate that N85°E is the optimal strike angle for 2-D inversion.

4.2.3 *Profile 3*

Profile 3 contains 12 unevenly distributed sites with six closely spaced sites in the northwest and six more sparsely spaced sites in the southeast. Based on the rms misfits (Fig. 5), the optimal geoelectric strike direction on the northwestern half of the profile is around N15°E. However, the misfit curves show that for these sites, a strike between N90°E and N80°E also produces a low misfit. This result shows that although the minimum misfit on Profile 3 corresponds

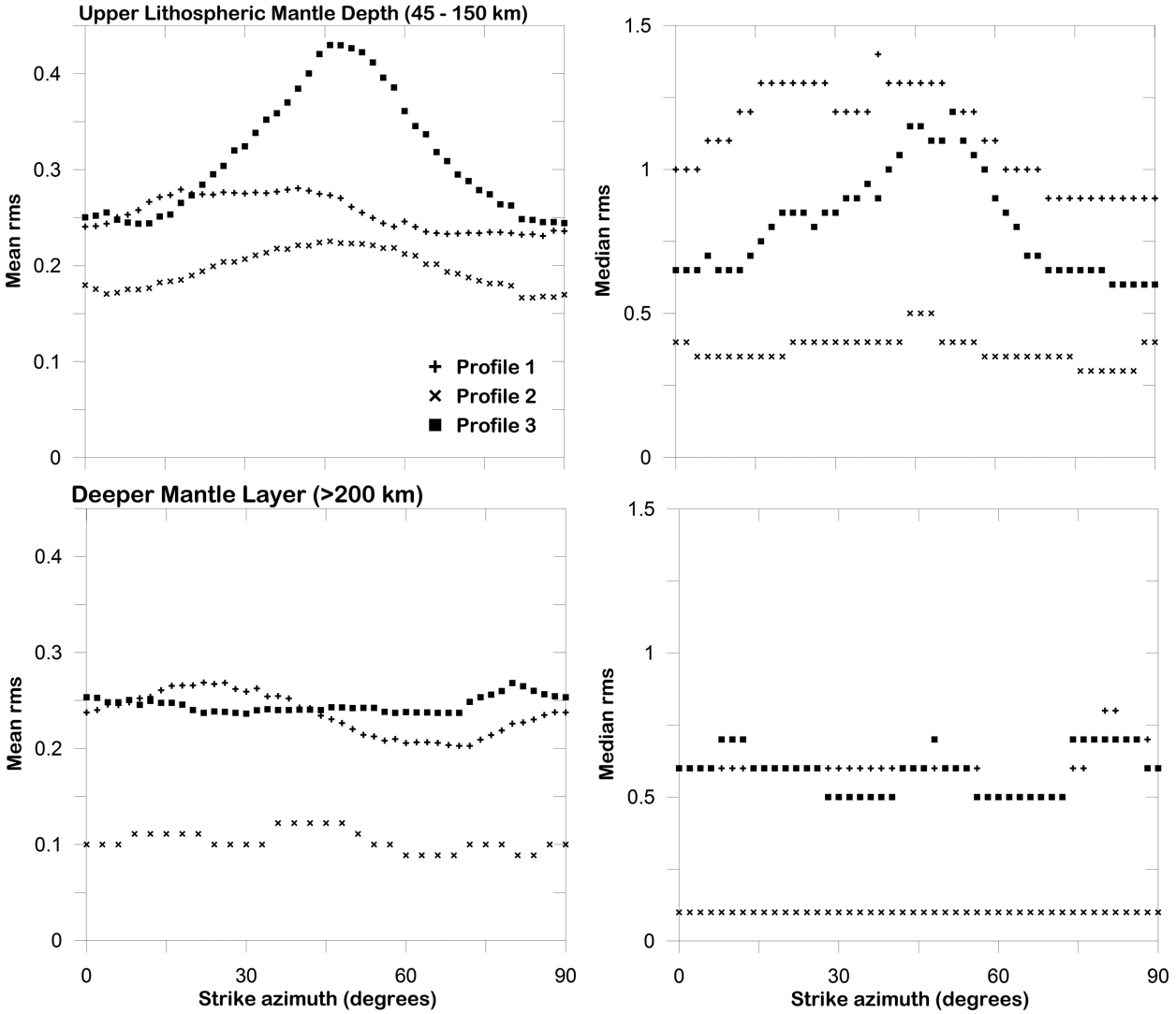

Figure 4. Misfit versus azimuth plots for robust misfit estimates. The plots show, as a function of regional strike azimuth, the minimum of the mean (left-hand panel) and median (right-hand panel) of the absolute value of the misfit determined in GB decompositions at individual sites. The final results are based on only those sites with rms misfit of <2.0.

Table 1. Summary of the geoelectric strike azimuths. Method 1 is the azimuth derived from the multi-frequency multi-site GB–MJ decomposition, Method 3 is the azimuth based on the minimum mean absolute error at each site and Method 4 is the azimuth based on the median absolute error at each site. The table also shows the final azimuth adopted for 2-D inversions used to obtain the lithospheric mantle resistivity structure and the earlier result from Mareschal *et al.* (1995).

	Upper lithospheric mantle layer				Deeper mantle layer		
	Profile 1	Profile 2	Profile 3	Profile 4	Profile 1	Profile 2	Profile 3
Mareschal	N80°E ± 6°						
Method 1	N85°E	N85°E	N86°E	N8°W	N62°E	N57°E	N67°E
Method 3	N80°E ± 10°	N85°E ± 4°	N84°E ± 5°	–	N65°E ± 5°	N65°E ± 5°	N62°E ± 5°
Method 4	N80°E ± 10°	N80°E ± 6°	N85°E ± 5°	–	N65°E ± 6°	All angles	N65°E ± 6°
Final	N85°E	N85°E	N85°E	N8°W		N65°E	

to strikes that are oblique to those on Profile 1, it is possible to fit the observations reasonably well with a common strike azimuth. The differences observed in the minimum misfit results may be caused by a subtle difference, such as a residual influence of crustal strike effects in the Profile 3 results. Within the southeastern CGB and CMB, the results suggest an upper lithospheric mantle strike angle in the N90°E and N80°E azimuthal range. The misfits are generally high for sites LITM05 and LIT026 when compared with other sites along the profile, and these sites were eliminated from further geoelectric strike analyses.

The MJ-GB strike determined for this profile is N86°E. The E_2 and E_3 misfit curves indicate results of 84° ± 5° and 85° ± 5°, respectively in good agreement with the MJ-GB value. The results for Profile 3 indicate that N85°E is an appropriate strike angle for 2-D inversion meaning that a common azimuth can be used for modelling all three profiles north of Lake Ontario.

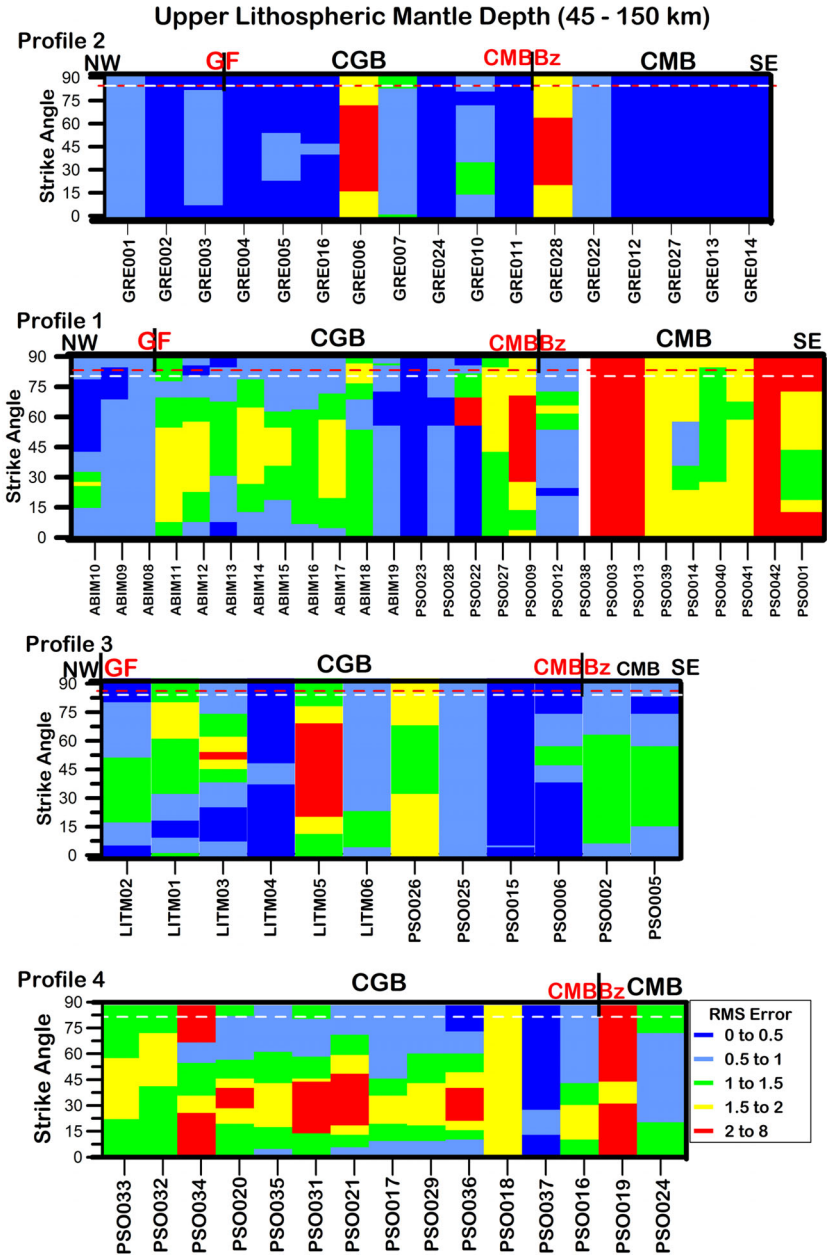

Figure 5. The rms misfit for single sites versus strike azimuth for a GB fit to the upper lithospheric mantle depth band (45–150 km) for Profiles 1–4. Results are plotted in order of the position of each site on the profile but the intersite distance is not preserved. The red dashed line is the regional strike azimuth of the profile based on the GB–MJ multisite multifrequency analysis and the white dashed line is based on the minimum misfit of the two more robust misfit measures. The gap in Profile 1 indicates the absence of data for this depth range at that site.

4.2.4 Profile 4

The strike direction for Profile 4 was determined using only methods 1 and 4. The rms misfit for the lithospheric mantle depth band (Fig. 3) has a relatively complex form. Several sites show high levels of misfit at all strike azimuths: PSO019 and PSO034 show high (>2) rms misfit distribution for this depth range and PSO018 is characterized by misfit values of between 1.5 and 2. Many of the remaining sites show a high rms misfit at azimuths between N10°E and N30°E indicating that an appropriate regional strike is excluded from this azimuthal range. In contrast, a geoelectric strike azimuth between N35°E and N90°E seems appropriate for many sites along the profile. Following the elimination of some sites with high rms misfit and galvanic distortion (PSO019, PSO020, PSO029 and PSO034) the MJ-GB multisite multiperiod analysis produced a result of N82°E for the whole profile.

The inherent 90° ambiguity in strike azimuth determination was resolved by choosing the direction closest to the strike of the large-scale geological features in the study area, which is N8°W. This choice is consistent with observations farther to the northeast. At that location, the large-scale trend of the Grenville Front and CMBBZ is closer to east–west and strike analyses yield an azimuth close to this value. It is of note that the phase tensor results for a number of sites on Profile 4 (Adetunji 2014; Adetunji *et al.* 2015) indicate that the azimuth of N8°W corresponds to the minor axis of the phase tensor or the more resistive direction (e.g. Hamilton *et al.* 2006).

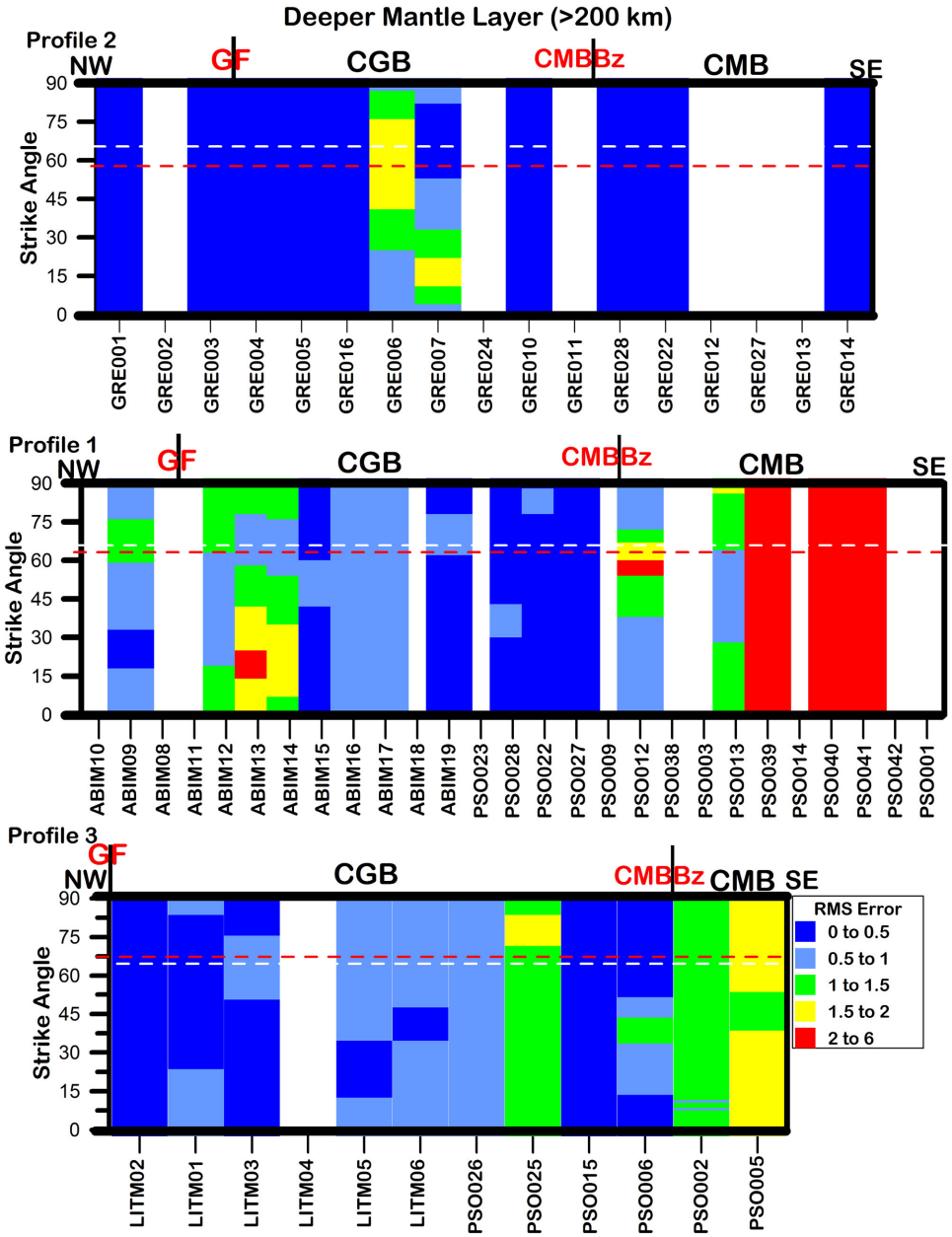

Figure 6. The rms misfit for single sites versus strike azimuth for a GB fit to the deeper mantle depth band (>200 km) for Profiles 1–3. The red dashed line is the regional strike azimuth of the profile based on the GB–MJ multisite multifrequency analysis and the white dashed line is based on the minimum misfit of the two more robust misfit measures. The gaps in the results indicate the absence of data for this depth range at the corresponding sites.

4.3 Common strike azimuth for the deeper mantle layer

The strike direction in deeper mantle layer range is determined mainly for the purpose of comparing the geoelectric strike results with other information such as the absolute plate motion (APM) directions. Fig. 6 shows the individual site misfit versus regional strike for this depth range along Profiles 1, 2 and 3. The plot includes a number of sites with missing data corresponding to sites in which there are no responses with equivalent Niblett–Bostick depths larger than 200 km. There is no data for this depth range on Profile 4 due the presence of conductive Upper Ordovician shale which limits the resolution of MT method in the crust and deeper mantle lithosphere.

The rms misfit distribution of Profile 1, for the deeper mantle depth range (Fig. 6), shows that the regional strike is defined mainly by sites in the CGB. The data from the CMB is characterized by high rms misfits, and there is no distinct strike direction defined in this region. The MJ–GB multisite multifrequency analysis yields an optimal direction of N62°E for the whole profile, and minimization of the more robust measures of misfit yields values of N65°E ± 5° and N66°E ± 5° for Methods 3 and 4, respectively.

The data from only 11 sites from Profile 2 penetrate to deeper than 200 km and, as observed at upper lithospheric depths; the corresponding GB misfits are characterized by very low values and low sensitivity to the regional strike azimuth, likely due to large errors on the impedances. However, the results from Methods 2 and 3 do define an overall strike angle that is in good agreement with that found for Profile 1. The MJ-GB multisite multifrequency analysis produces an optimal strike direction of N57°E for the whole profile, and Method 3 produces a strike of N65°E with an uncertainty

of 5°. For this data set there was no significant dependence of the Method 4 misfit measure with azimuth.

For Profile 3, the rms misfit of the distortion model is generally low for the CGB section of the profile but exceeds 1.0 for the CMB section. This observation suggests that a wide range of strike azimuths provide adequate GB fits to the CGB section of the profile. The MJ-GB multisite, multifrequency analysis yields an optimal strike direction of N67°E for the whole profile. Method 3 yields an azimuth of N62°E ± 5° and Method 4 yields a result of N65°E ± 6°.

For each profile, the result of the overall strike for deeper mantle depth range is defined with greatest resolution for Profile 1 and with least resolution for Profile 2. The result shows very good agreement across the whole study area and indicates an overall strike azimuth of N65°E.

5 2-D INVERSION

5.1 Preparation of data sets for inversion

Prior to 2-D modelling and inversion, MT datasets for each profile were prepared by decomposing them to the regional geoelectric strike azimuths. This was done by fitting the regional impedances derived from the GB decomposition with the regional geoelectric strike azimuth constrained to the upper lithospheric mantle value of N85°E for Profiles 1–3 and N8°W for profile 4. Note that the data were not rotated, but were fit to an appropriate model of distortion with the defined strike angle. Such model fitting yields far superior results than rotation alone (Jones & Groom 1993; McNeice & Jones 2001).

In 2-D, the MT responses formally decouple into two independent modes of induction and are termed the transverse electric (TE) and the transverse magnetic (TM) modes. For the TE mode, the electric field is parallel to the geoelectric strike, and for the TM mode it is perpendicular. The TE mode is sensitive to along-strike current flow, which is dictated by the conductance of conductive regions of the model, but provides lower resolution of the lateral position of structures than TM. The TM response is primarily sensitive to charges on conductivity contrasts or gradients of lateral boundaries. Inclusion of both modes in the inversion, which is formally a joint inversion due to the decoupling of Maxwell's equations into two independent sets, allows for superior determination of the subsurface resistivity structure. 2-D inversion methods are sometimes applied to MT data containing weak 3-D effects. When the conductive features in a model have a finite strike length, the TE response is generally more distorted than the TM response and this necessitates the weighting of the 2-D modelling heavily towards the TM response (Jones 1983; Wannamaker 1999; Ledo *et al.* 2002; Ledo 2005). There are some structures for which the TM mode is more affected by 3-D effects than the TM mode (e.g. Park & Mackie 1997), so one must be cautious when only modelling the TM mode.

5.2 Inspection of the pseudo-sections for qualitative information

Prior to the actual geophysical inversions the data were edited and examined using TE and TM pseudo-sections. For 1-D and 2-D structures, the impedance phase responses are related to the gradient of apparent resistivity with log period (e.g. Parker & Booker 1996; Weidelt & Chave 2012). Consistency between apparent resistivity and phase responses at individual sites was checked using the D+ approach of Parker (1980), as implemented in the WinGLink software. This method performs 1-D modelling of the admittance which identifies unreliable data points that were subsequently removed prior to modelling and inversion.

The final MT phase and apparent resistivity pseudo-sections for the four profiles are shown in Figs 7 and 8. MT pseudo-sections for Profile 1 are presented and discussed in Adetunji *et al.* (2014) but are included here for comparison with the pseudo-sections for the other profiles. Examination of the TE and TM apparent resistivity and phase responses shows that there are significant differences between these modes along both profiles providing an indication that 2-D structures exist in the subsurface along both profiles.

All of the profiles display phase responses with low phases at shorter periods and higher phases at long periods. On Profile 1, a period band of very high phase responses (>70°) centred on 10 s period extending along the entire length of the profile (Fig. 7) reflects the transition from high apparent resistivity at intermediate periods to lower apparent resistivity at long periods (Fig. 8). This response defines the decreased resistivity observed at 150 km depth in the resistivity model (Fig. 2). Profiles 2 and 3, exhibit a less pronounced increase in phase (>50°) centred on 1–10 s period indicating the presence more resistive structures in the mantle lithosphere. However, a localized increase in the TM phase response (to >70°) at 1–10 s period in the middle of Profile 3 does suggest locally decreased resistivity. The increased phase observed at the longest periods (>100 s) on Profiles 2 and 3 provides an indication of an increase in conductivity at depths corresponding to the maximum penetration of the signal. For Profile 4, the band of low phase at the shortest periods is more prominent than at the other sites and is associated with the higher conductance of the surface sedimentary rocks beneath that profile.

The pseudo-sections provide additional information on the resistivity structure in the CMB. The MT response at the southeast end of Profiles 2 and 1 and at the east end of Profile 4 includes a zone of increased TE and TM phase (>70°) at intermediate periods providing evidence for a lithospheric conductor at these locations. The phase pseudo-sections for Profiles 2 and 3 show the high phase response observed at short periods occurs at progressively longer period with increasing distance into the CMB providing evidence for a southeast dip of the upper surface of a resistive zone in the lithosphere.

5.3 2-D inversions

In this study we used the 2-D isotropic modelling and inversion algorithm of Rodi & Mackie (2001) as implemented in Geosystem's WinGLinK software. The software uses a finite difference numerical method for forward modelling and the non-linear conjugate gradient (NLCG) method for inversion. NLCG implements direct iterative minimization of an objective function that penalizes data residuals and second spatial derivatives with respect to resistivity structures (Rodi & Mackie 2001, 2012).

The inversion models were obtained by solving for the smoothest model using uniform-grid Laplacian regularization and minimizing the integral of the Laplacian (Rodi & Mackie 2012). The range of possible models that could fit the data was explored by running several 2-D inversions using different combinations of inversion parameters (both regularization and smoothing parameters) and data. Final 2-D models were obtained by fitting both TE and TM data for all the sites using a 100 Ωm half-space as the starting model. The standard deviation error on each data point was set to either the

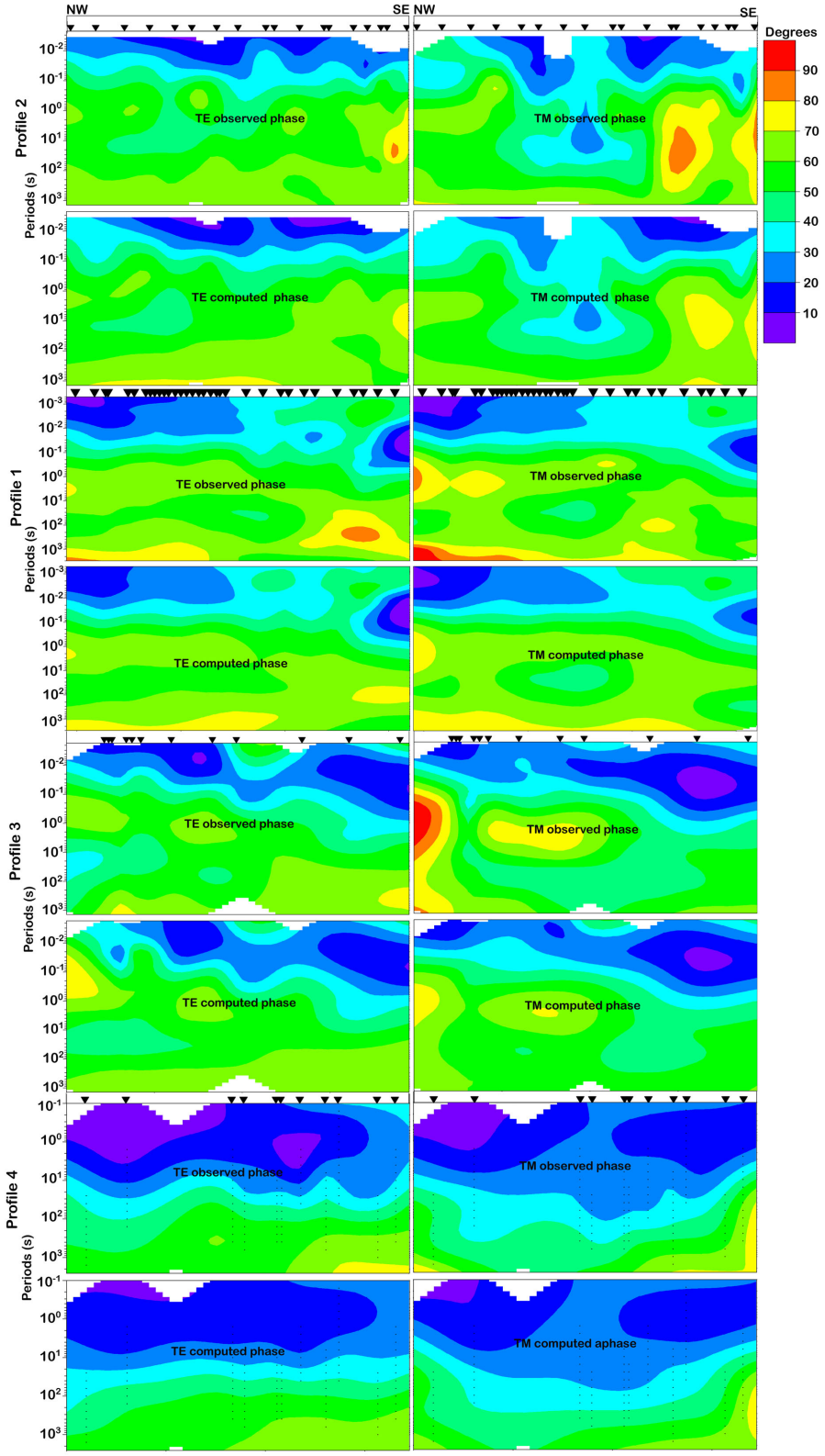

Figure 7. Phase pseudo-sections of TE and TM responses for Profiles 1–4. The observed data are the regional MT responses derived from the GB decomposition using the upper lithospheric mantle strike azimuth of N85°E for Profiles 1–3 and N8°W for Profile 4. Panels show the observed responses and the responses of the 2-D resistivity model fitted to the observed data. Fig. 1 shows the spatial distribution of the sites.

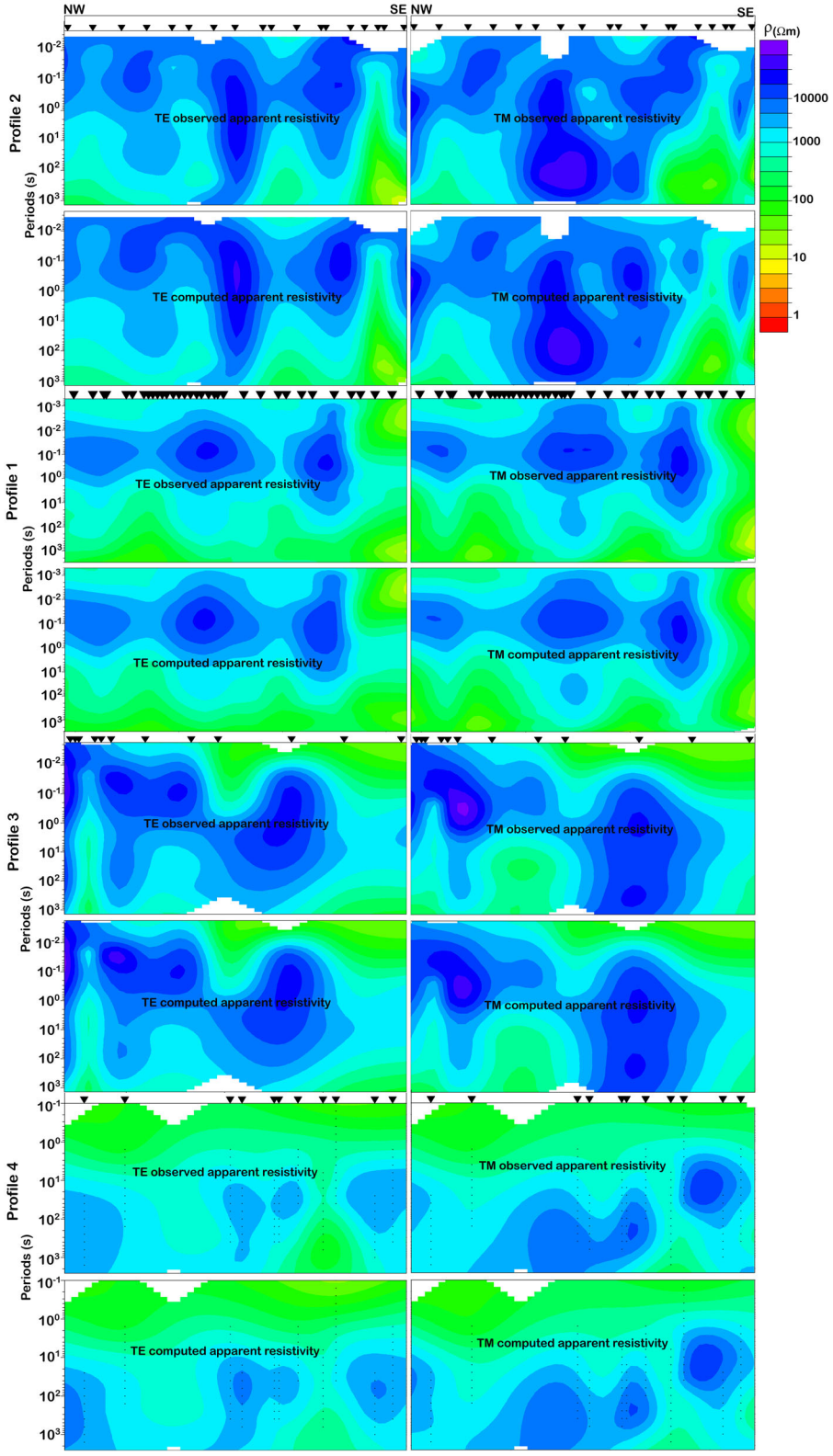

Figure 8. Apparent resistivity pseudo-sections of TE and TM responses for Profiles 1–4. The observed data are the regional MT responses derived from the GB decomposition using the upper lithospheric mantle strike azimuth of N85°E for Profiles 1–3 and N8°W for Profile 4. Fig. 1 shows the spatial distribution of the sites.

calculated error values or to an error floor, whichever one is the larger. For the initial set of inversions, the apparent resistivity error floors were set at 60 per cent for both modes, the TE phase error floor was set at 30 per cent and the TM phase error floor at 5 per cent. The apparent resistivity was down-weighted in order to reduce the effect of static shift in the inversion. These floors emphasize the fit to the TM phase, and yield an appropriate model that served as the start model for the next inversion step. All the error floors were subsequently reduced to 20 and 16 per cent for TE and TM resistivity and 5 per cent ($\sim$1.2°) and 4 per cent ($\sim$1°) for TE and TM phases. Thus again the TM data were prioritized over the TE data. At the beginning of every new inversion, the inversions were based on an interpolated data set with five frequencies per decade (in order to decrease the execution time) but the data set was changed to the actual station data, through restarting, as the inversion progressed. For a more reliable final model with deeper minimum of the objective function, all inversions were restarted at least once after their initial termination. The typical number of iterations per sequence ranges from 400 to 600, and the number of sequences was 6–10 depending on final models. During the inversion procedure the static shift was corrected by running a sequence of inversions with the TE or TM mode static shift for all of the sites, or for a subset of the sites, included as inversion parameters. The average static shift values for TM mode for Profiles 1, 2, 3 and 4 are 1.3, 0.8, 0.9 and 1.1, respectively. The corresponding values for the TE mode are 1.4, 1.65, 1.1 and 1.2.

Exploring for the optimal model involves the use of different combinations of weighting functions and regularization parameters (e.g. Mackie *et al.* 1997; Spratt *et al.* 2009; Matsuno *et al.* 2010; Schäfer *et al.* 2011). Parameters such as the Tikhonov regularization parameter (τ), horizontal derivative (α), depth function (β), horizontal smoothing (H) and vertical smoothing (V) factors were examined to explore for the optimal model. Following this examination, for the final inversion models, the weighting function parameters were set at $\alpha = 1$, $\beta = 0.3$, $H = 500$ and $V = 500$ for both profiles while $\tau = 3$ and 6 were used for Profiles 2 and 3, respectively. These values were chosen after a series of initial inversions were performed to determine the best smoothing and regularization parameters, using an L-curve approach (Hansen 1992).

The inversion results for each of the profiles are shown in Fig. 9. The crustal part of the resistivity model are not considered here as the optimal crustal models are derived using a different strike angle from the azimuth that is most appropriate for the upper lithospheric mantle. The description of the model for Profile 1 and the corresponding fit to the data are presented in Adetunji *et al.* (2014) and are not repeated here. The models contain a number of common features: a large-scale resistive zone in the upper mantle lithosphere (labelled R in Fig. 9), enhanced conductivity in the mantle lithosphere beneath the CMB (labelled C1), and enhanced conductivity below the large-scale resistor and in gaps in the resistive zone (labelled C2).

Fig. 9(a) shows the mantle resistivity model obtained for Profile 2 together with site-by-site data misfits. The northwest half of the model shows a relatively good fit to the data, with acceptable rms misfit values that are mostly <2. However, to the southeast of the CMBBZ, the fit becomes poorer as most sites consistently show values closer to 2.The global rms misfit of the final mantle resistivity model is 1.6. The pseudo-section response of the model shows a good fit of the model to all of the major data features. The inversion model reproduces all of the large-scale features in the observed data (Figs 7 and 8).

The resistivity model for Profile 2 is dominated by a large-scale resistive region, labelled R, which extends laterally from the Pontiac subprovince into the middle of the CMB. This is a very well resolved feature, defined by 13 MT sites, that extends from $\sim$70 km depth to a maximum of $\sim$300 km depth in the centre of the CGB. Its resistivity is 3000–20 000 Ω.m. The lithospheric resistor lies along strike from a resistive region in the upper mantle lithosphere on Profile 1. The top of the resistive zone is at a similar depth in both profiles. On Profile 1 it has a clear southeast dip and increases in depth from $\sim$50 km, in the middle of the CGB, to $\sim$120 km at its southeastern extent. For Profile 2 there is also some indication that the top of the feature has a southeastern dip as it again increases in depth from $\sim$40 km, in the CGB, to $\sim$120 km at its southeastern extent. However, further to the northwest the upper 100 km of the resistivity structure is more complex and includes some conductive regions. As anticipated from examination of the phase pseudo-sections (Fig. 7), the resistor extends to much greater depths on Profile 2 than on Profile 1 where its base is at a depth of $\sim$150 km.

The mantle lithosphere in the southeastern end of Profile 2 (labelled C1), beneath the CMB, is relatively conductive (mostly <100 Ω m). On both Profiles 1 and 2, the southern margin of the resistive lithosphere is approximately 100 km southeast of the CMBBZ.

The mantle resistivity model for Profile 3, along with misfits for individual sites, is shown in Fig. 9(c). The average site rms misfit for sites close to the GF is around 2, and this may be as a result of the closeness of the sites in this region. Other sites along the profile show good fit to the data, with values mostly <1. The model provides a very good fit to the data with a global rms misfit of 1.4. Examination of the pseudo-section responses shows that all of the main features in the observed responses are reproduced. The model responses slightly underestimate the high phase anomaly observed at intermediate periods in the central CGB.

The resistivity model along Profile 3 is again dominated by a large-scale resistor (labelled R in Fig. 9c) that extends from 80 to 280 km depth with a resistivity of 3000 to over 20 000 Ω m. This feature is defined by the data from a number of the sites along this profile. As on Profiles 1 and 2, the southeastern margin of the resistor again occurs at a location about 100 km southeast of the CMBBZ. In contrast, though to the mantle resistivity models for Profiles 1 and 2, the resistor is separated into two parts by a conductive (500 Ω m) region in the central CGB. This feature is clearly supported by the observation of a phase anomaly at $\sim$1 s period in this location (Fig. 7) and by decreased apparent resistivity observed at longer periods (Fig. 8). It also appears in early iterations of the inversions, regardless of the parameters or starting model used. The upper 120 km of the Profile 3 resistivity model is more complex than at the same depth range in the models for the other profiles. It includes a conductive region within the northwest part of the CGB and a resistive zone in the southern CGB and CMB.

Fig. 9(d) shows the mantle resistivity model and data misfit for Profile 4. Sites PSO020, PSO029, PSO031 and PSO034 were excluded from the final set of inversions because they exhibited high rms misfit (>4) in earlier sets of inversions. The global rms error of the final resistivity model is 1.47 and the fits of the inversion model to individual sites are spatially uniform. In addition, the large-scale features in the observed data are all reproduced by the model response as shown by the pseudo-sections in Figs 7 and 8.

The resistivity model for Profile 4 shows that the lithospheric mantle in the northeast part of the profile is relatively conductive with a resistivity of 100–200 Ω m decreasing to values of <5 Ω m in a conductor beneath the CMB (labelled C1). There are resistive

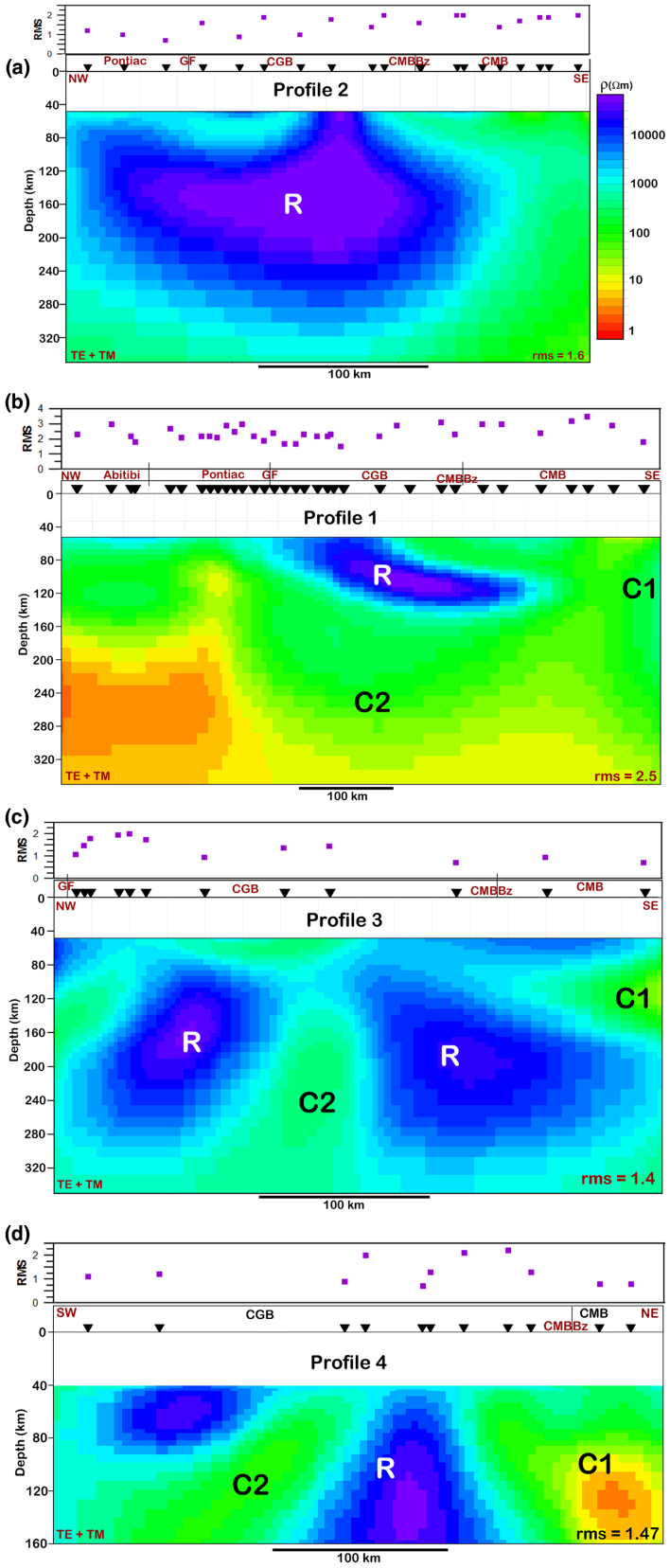

Figure 9. Resistivity models derived by joint inversion of TE and TM responses of Profiles 1–4 (a–d) for the lithospheric data set (V.E. = 0.5). The rms misfits of the joint TE and TM (purple squares) inversions at individual sites are plotted above each inversion model. The crustal section (upper 48 km) of the model is not shown.

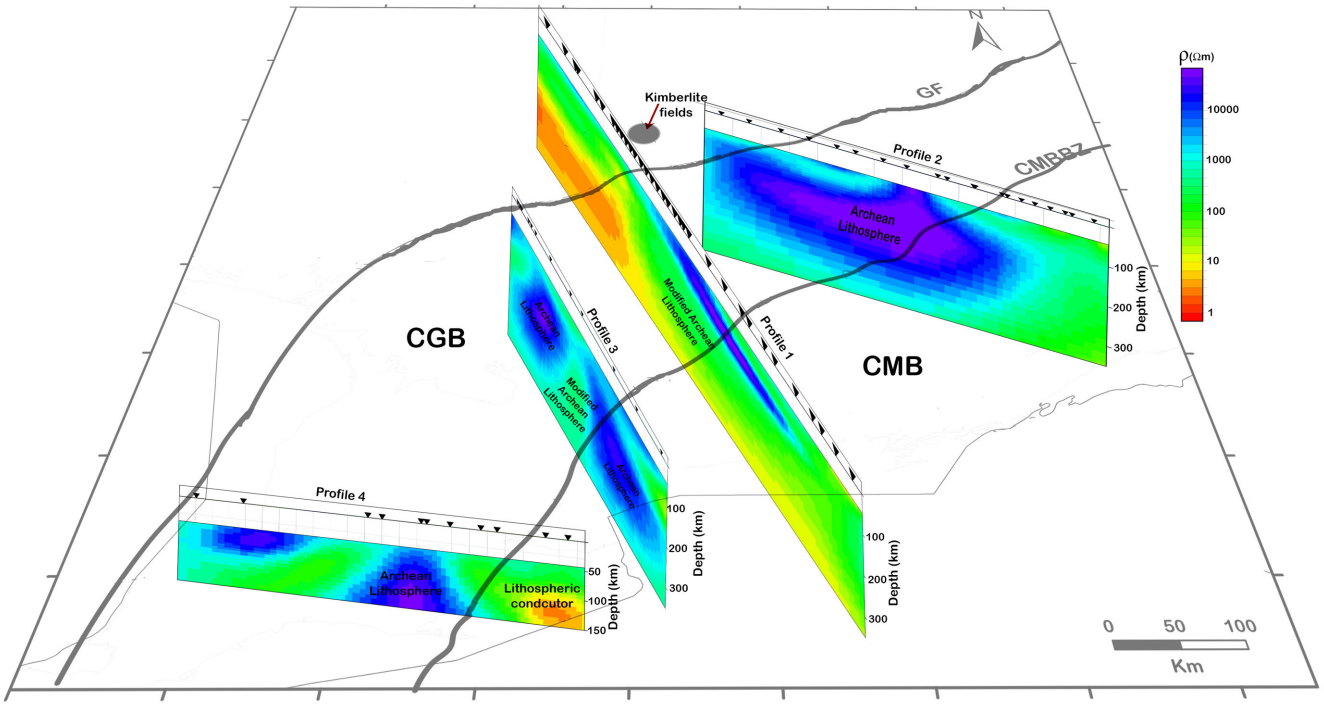

Figure 10. Resistivity models of Profiles 1 (Adetunji *et al.* 2014), Profiles 2–4 projected onto the map of the study area. The models, with V.E. = 0.5 and depth extent of 350 km for Profiles 1–3 and 150 km for profile 4, are aligned with the MT data sites. The crustal section (upper 48 km) of all the models is not shown.

blocks in the middle and southwest parts of the model. Beneath the northeastern CGB a resistive zone (labelled R), containing resistivity values of >2000 Ω m extends from the base of the crust to depth of at least 150 km. A second resistive block to the southwest extends from the base of the crust to about 90 km depth. The resistivity of the lithosphere beneath this block and between the two resistive blocks is between 200 and 500 Ω m (labelled C2).

The resolution of the resistivity models, and particularly of the large scale resistor in each model, was assessed through examination of signal penetration and through hypothesis-testing of alternative models, as described below. Adetunji *et al.* (2014) describe a similar analysis for Profile 1. Examination of the equivalent Niblett–Bostick depths for responses on Profiles 2 and 3 demonstrates that there are a number of sites with penetration to the base of the resistors. The resistors are defined by an increase in apparent resistivity, and corresponding decrease in phase, at intermediate to longer periods (Figs 7 and 8). The base of the resistor is defined by an increase in phase at the longest periods (>100 s) and, as noted above, the gap in the middle of the resistor on Profile 2 is defined by a decrease in apparent resistivity and corresponding increase in phase at shorter periods. The results of Profile 4 show that the conductor C1 and the resistor R are first-order features that exist in the subsurface. The conductor is associated with an increase in the TE and TM phase responses at longer periods (Fig. 7). Modelling indicates that although the geometry of the individual resistive blocks is not well resolved; the two blocks are definitely separated by more conductive lithosphere. The MT data are unable to resolve the depth to the base of either the resistor R or conductor C1. Finally, inversions were re-run using starting models based on the inversion results, but with the resistive zones replaced by more conductive zones. Even when the minimization norm was set to return the model closest to the starting model, the models obtained still included the resistors, indicating that they are data-supported structures.

6 DISCUSSION AND INTERPRETATION

Fig. 10 synthesizes the resistivity results and shows the large-scale variations in resistivity structure across the Grenville Province. In order to allow for improved tectonic interpretation, the models are plotted at the location of the MT sites rather than the location of the projected 2-D modelling profiles. The results show several common features in the resistivity models, including resistive upper mantle lithosphere beneath the northwest Grenville Province and more conductive lithosphere beneath the CMB. However, they also exhibit variations including a shallowing of the base of the resistive lithosphere beneath Profile 2 and gaps in the resistive lithosphere on Profiles 3 and 4. The geometry of these large-scale 3-D features will be able to be confirmed and refined slightly by 3-D inversion of the MT data sets. However, as indicated by the dimensionality analyses, the analysis of the data fit of the 2-D resistivity models, and by additional 2-D inversions using a range of strike azimuths, the main features of the models are well resolved by the 2-D inversions. It is very significant to note that the three primary features of the large-scale structure: the resistive upper lithosphere, more conductive underlying mantle, and the conductive CMB lithosphere can all be recognized and mapped in the MT phase responses.

6.1 Conductive mantle lithosphere beneath the CMB

Fig. 10 shows that on all four profiles, to the south of the resistive mantle lithosphere, beneath the CMB, the lithosphere of the Grenville Province is relatively conductive. This region hosts localized conductors on Profiles 1 and 4. On Profile 4, the conductor has its top at ∼100 km depth and with resistivity values <5 Ω m. Adetunji *et al.* (2014) model a conductor at the southeastern end of their profile, Profile 1, approximately 200 km south of the CMBBZ. This conductor has its top at ∼100 km depth and contains resistivity

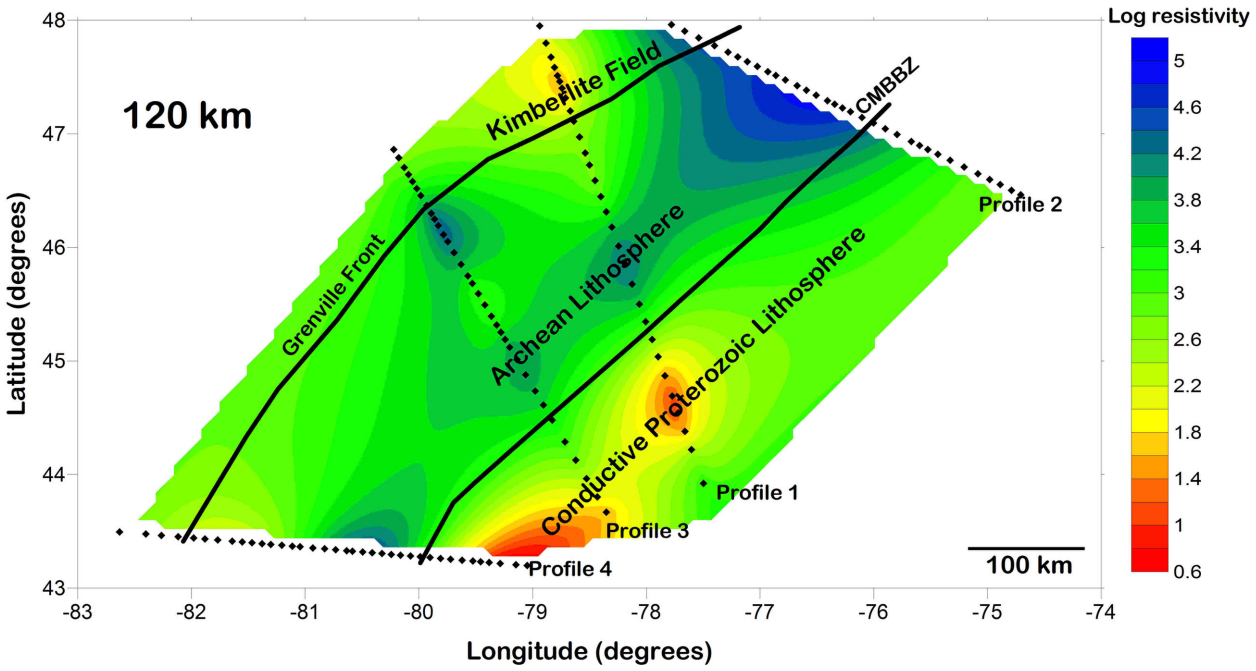

Figure 11. A horizontal slice, at 120 km depth, through the resistivity models of Profiles 1–4. The resistivity values at this depth, interpolated with natural neighbour algorithm, were projected onto the MT data acquisition profile and contoured. The result shows lateral extension of Archean lithosphere throughout the study area. It also shows conductive Proterozoic lithosphere extending across all four profiles and localized lithospheric conductors on Profiles 1 and 4.

values $<10\ \Omega$ m. Figs 10 and 11 show the geometrical relationship between the conductors in the two studies. The 2-D MT inversions for Profiles 2 and 3 also suggested the presence of deep conductors beneath the CMB. However, these features were located beyond the final site in each profile and their resolution was considered inadequate for them to be examined in detail.

The observations establish the presence of conductive lithosphere beneath the CMB in the Grenville Province. As shown in Figs 10 and 11 the conductive lithosphere appears to be continuous along strike for at least 100 s of kilometres. The top of localized conductors within this zone is at a depth of around 100 km and based on the results for Profile 1 the base is at a depth of around 160 km. This depth distribution provides an indication that anomalies may be due to the presence of grain boundary graphite films (Selway 2014). Such anomalies would be expected to have a base at around 150 km depth in stable continental lithosphere at the limit of the graphite stability field.

Adetunji *et al.* (2014) interpret conductive features northwest of the CMB in the Grenville Province as being associated with the deep effects of the passage of the postulated Great Meteor hotspot (Crough 1981; Sleep 1990) and kimberlitic magmatism. A subvertical conductor beneath the Pontiac subprovince occurs only a few tens of kilometres along strike from the diamondiferous kimberlites in the Kirkland Lake and Cobalt kimberlite fields (Adetunji *et al.* 2014). One explanation for the localized anomalies at 100–150 km depth in the CMB is that they are also associated with kimberlitic magmatic processes. It has been shown that kimberlite melts are normally rich in carbon and are likely to release carbon dioxide in the uppermost mantle (Hunter & McKenzie 1989; Pearson *et al.* 1994; Sleep 2009). The degassed carbon dioxide could move along grain boundaries (Hunter & McKenzie 1989) and become converted to graphite, which is stable at depths less than 150 km (Pearson *et al.* 1994). However, it unclear whether these processes can occur over a sufficiently wide spatial scale to explain conductive anomalies on profiles separated by 300 km.

It is probable that conductive nature of the deep lithosphere beneath the CMB could be due, at least in part, to the introduction of water and carbon into the mantle during pre-Grenvillean (1450–1740 Ma) collisional events and subduction (Carr *et al.* 2000). This mechanism would provide the source for widespread introduction of elements capable of enhancing conductivity. It is of note that in the southern United States, the Grenville suture is associated with enhanced lower crustal and upper mantle conductivity (Ogawa *et al.* 1996; Wannamaker *et al.* 1996; Wannamaker 2005) suggesting a very large-scale distribution of conductive lithosphere. Other Proterozoic suture zones are also associated with enhanced conductivity at crustal and/or mantle depth (e.g. Korja & Hjelt 1993; Boerner *et al.* 2000; Jones *et al.* 2005; Heinson *et al.* 2006; Spratt *et al.* 2009). Carbon and water introduced during the pre-Grenvillean tectonic activity may have formed an important source during the Cretaceous kimberlitic activity which, as noted above, may have produced the localized conductive anomalies observed in the lithosphere of the CMB. However, it is also conceivable that these anomalies may have formed during the pre-Grenvillean tectonism.

6.2 Resistive mantle lithosphere beneath the Grenville Front and CGB

The most striking feature on the MT models is the southeast-dipping resistive lithosphere that extends from the base of the crust to a depth of ~280 km in Profiles 2 and 3, to ~150 km in Profile 1and to at least 150 km in Profile 4. The resistor extends laterally from the Superior Province into the centre of the CMB in the Grenville Province. In earlier MT studies of Profile 1 (e.g. Mareschal *et al.* 1995; Adetunji *et al.* 2014), the resistor was interpreted to be an extension of Archean Superior mantle lithosphere beneath the northeastern Grenville Province. The resistor is associated with a zone of high seismic velocity between 50 and 150 km depth in which the *S*-wave velocity reaches values up to 10 per cent higher than global models

(Chen & Li 2012) supporting the idea that it represented highly depleted continental lithosphere. Adetunji *et al.* (2014) compared the resistivity within the feature to 2-D resistivity models from southern Africa and showed that the modelled resistivity is comparable to that in lithosphere beneath the Archean Kapvaal craton.

The new 2-D resistivity models for Profiles 2–4 provided in this study show the resistor extends along strike for at least 800 km (Figs 10 and 11), and includes resistivity values exceeding 20 000 Ω m over this whole region. The models from all four profiles also show that the resistor extends 300 km southeast beneath the Grenville Province from the Grenville Front to a point about 100 km southeast of the CMBBZ.

The along-strike extent of the resistor is a factor that must be included in its interpretation. To the northeast, the resistive lithosphere beneath the Grenville Province was interpreted as being associated with the adjacent Superior Province (Adetunji *et al.* 2014). However, farther to the west the Grenville Province truncates younger rocks of the Early Proterozoic Southern Province, and farther southwest, it truncates progressively younger rocks including those deformed during the Penokean orogeny (e.g. Forsyth *et al.* 1994), and Mazatzal orogeny (Whitmeyer & Karlstrom 2007). Based on the similarity of the resistor along strike it is more likely that it represents a coherent block of Archean lithosphere rather than being composed of Archean rocks in the northeast and Proterozoic rocks to the southwest. We therefore interpret the mantle lithosphere beneath the entire Grenville Province as being part of the Superior lithosphere. This interpretation implies that the Mazatzal mantle lithosphere does not extend into the Grenville Province. Additional support for this interpretation comes from shear wave splitting anomalies that show fairly consistent near east–west fast directions and ∼0.5 s time splits within the CGB of the Grenville Province in areas around Profile 4 (Frederiksen *et al.* 2006).

In all of the resistivity models, the southeast limit of the resistor has a wedge-like form, and the southeastern part of the resistor is overlain by more conductive lithosphere. We interpret the more conductive lithosphere to be Grenvillian-aged lithosphere thrust over the margin of the Superior lithosphere. This geometry is most clearly illustrated on Profile 1 for which the upper surface of the resistor has a clear southeast dip.

6.3 Conductive lower mantle lithosphere

This study has also provided important new information on the geometry of the base of the resistor. As previously noted, on Profile 1 the base of the resistor occurs at ∼150 km depth. On Profile 2, the base occurs at ∼280 km along much of the profile. On Profile 3, the bases of each of the two resistive blocks are at around 280 km depth but there is a gap between the blocks, in which either the base shallows significantly or the blocks are separated by more conductive mantle, whose nature is unknown at this time. It is suggested that the narrow zone of conductive mantle that separates the lithospheric resistors on Profile 4 is connected to the more conductive mantle that separates two parts of lithospheric resistor on Profile 3 and to the conductive lower lithosphere on Profile 1 (Fig. 10).

We interpret the observed 280 km depth of the base of the resistor on Profiles 2 and 3 to represent the base on the lithosphere in the region, and the relief in the lower part of the resistor to be caused by enhanced conductivity in the lower lithosphere. The ‘deeper mantle layer’ referred to herein can now be defined as a lower lithospheric layer. Adetunji *et al.* (2014) showed that the resistivity below the resistor on Profile 1 is less than that in some Proterozoic terranes in southern Africa. The enhanced conductivity beneath the resistor is therefore interpreted as refertilized lithosphere with the processes of refertilization introducing conducting elements into the lithospheric mantle, such as carbon (in various forms), sulphides and water. As shown by Adetunji *et al.* (2014) on Profile 1, the conductive zone is bounded to the northwest by a vertical anomaly located only a few tens of kilometres along strike from the Kirkland Lake and Cobalt kimberlite fields. We therefore interpret the conductive lower lithosphere on Profile 1 and the middle on Profile 3 as a zone that has been metasomatized by fluids associated with the Cretaceous kimberlitic magmatism. As pointed out by Selway (2014), refertilization of the mantle can lead to long-lived enhanced conductivity.

Fig. 12 compares a horizontal slice through the resistivity models at ∼180 km with the seismic tomography results of Chen & Li (2012) for the same depth. There is a very strong spatial correlation of the *S*-wave velocity and electrical resistivity over the study area. The maximum decrease in resistivity, of approximately three orders of magnitude is correlated with a 3 per cent reduction in the *S*-wave velocity. The surface wave tomography models show similar lateral variations at depths extending from 120 to 200 km and the resistivity models show similar patterns extending from 150 to 240 km (Fig. 10).

At a larger scale, the receiver function and SKS inversion studies of Abt *et al.* (2010), Yuan & Romanowicz (2010) and Yuan *et al.* (2011) suggest the existence of a two-layer lithosphere and a mid-lithospheric discontinuities (MLD) in areas near this study area. The structural boundary occurs at ∼150 km depth. In the seismic studies, the layer above the MLD is interpreted to be chemically depleted lithosphere and the lower layer to be a younger, less depleted, thermal boundary layer (Yuan & Romanowicz 2010; Yuan *et al.* 2011). The two-layer lithosphere resolved in the resistivity model for Profile 1 is consistent with the seismic models, but the combined results from the three profiles suggests the existence of significant spatial variations in the MLD and that in places it may represent a localized feature.

The geophysical results from this study provide strong evidence of refertilization of a large volume of the lower lithospheric mantle by the passage of fluids. Conductivity is enhanced over a depth range between 150 and 280 km and over a horizontal spatial scale of several hundred kilometres. Veeraswamy *et al.* (2012) make a similar interpretation of relatively conductive lower lithosphere of a large region of Dharwar craton in India. In this case, the craton is interpreted to have been refertilized during its passage over the Reunion hotspot approximately 63 Ma.

The enhanced conductivity in the Grenville Province is observed at a depth of more than 150 km, beneath the graphite stability field (Kennedy & Kennedy 1976). The absence of any surface gravity anomalies or surface topography mirroring the spatial variations in the base of the resistor suggests that the refertilization has produced minimal changes to the density and thermal properties of the lower lithosphere. We therefore interpret the enhanced conductivity to be associated with the presence of water in nominally anhydrous minerals (e.g. Karato 1990; Jones 1999; Hirth *et al.* 2000; Korja 2007; Muller *et al.* 2009; Jones *et al.* 2012, 2014; Selway 2014). It is possible to estimate the amount of water required to explain the observed resistivity. At a depth of 180 km, the average resistivity of the refertilized region at around 45.5° N on Profile 1 is 180 Ω.m (Fig. 12). The average crustal heat flow in the Grenville Province is 41 ± 10 mW m^{-2} (Pinet *et al.* 1991; Mareschal *et al.* 2000) and the corresponding lithospheric geotherm

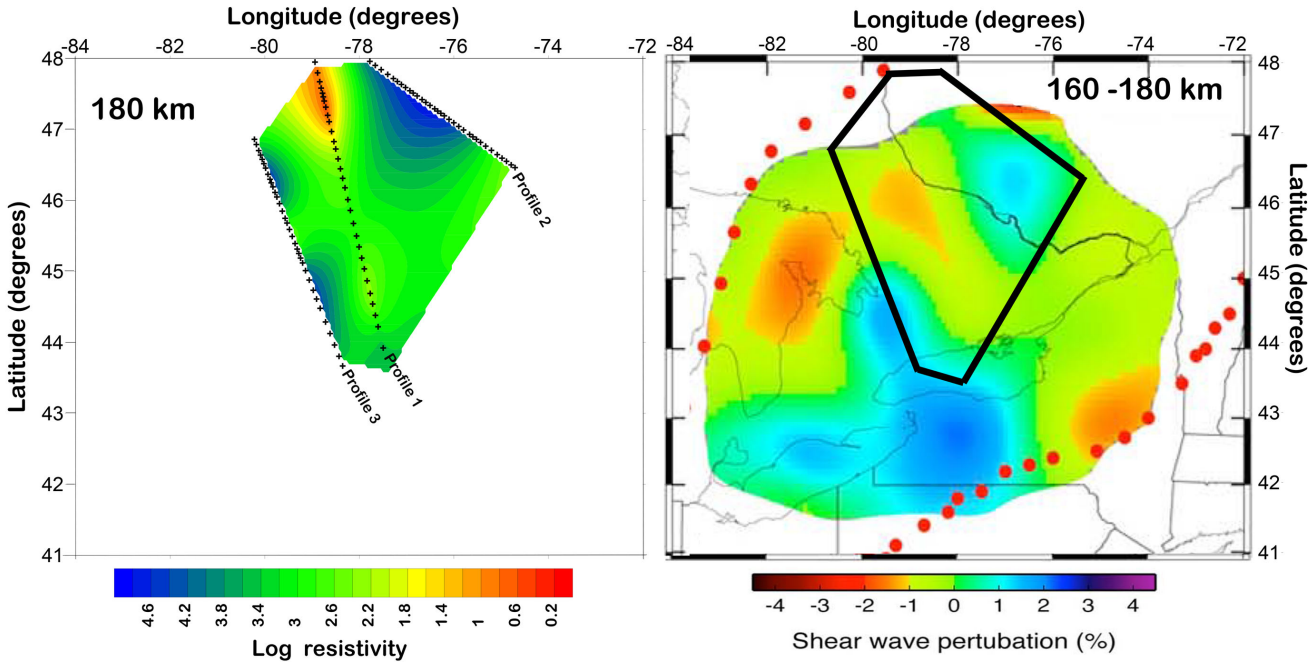

Figure 12. Comparison of electrical resistivity at 180 km depth with shear wave velocity perturbation (Chen & Li 2012). In order to produce the resistivity results the models for Profiles 1–3 were reprojected back to a line through the corresponding sites. Resistivity values extracted from the models at a depth close to 180 km were interpolated using a natural neighbour algorithm and then the results were contoured. The aerial extent of the resistivity model is shown by the black polygon on the seismic model. The resistivity results show good spatial correlation with the *S*-wave velocity model with the lowest resistivity values at 180 km depth corresponding to ∼−1.5 per cent velocity perturbation and the highest resistivity values at this depth corresponding to ∼+1.5 per cent velocity perturbation.

model of Artemieva (2006) indicates a temperature at 180 km depth of 1220 °C. Noting the dominance of olivine in the lithospheric composition, and that the laboratory conductivity estimates for olivine lie in the middle of the results for ortho- and clinopyroxene and garnet, the olivine resistivity–temperature relationship is used to convert from resistivity to temperature. Using the relationship of Jones *et al.* (2012, 2014), the resistivity of 180 Ω m and temperature of 1220 °C indicate a water content of 50 wt ppm. There is some uncertainty in this estimate associated with the resolution of the resistivity value in the MT inversions and the spatial variations in the resistivity in the models, as well as with the estimate of the temperature and the resistivity–temperature–water content relation. The alternative laboratory-based resistivity-water content model of Karato (1990) suggests lower water content whereas the models of Poe *et al.* (2010) and Yoshino *et al.* (2009) indicate a water content that is a factor of about four higher than that of Jones *et al.* model (Jones *et al.* 2012). However, the Jones *et al.* (2012, 2014) model used in our calculations is based on both laboratory and geophysical constraints so the present result is interpreted to provide a firm indication of a water content of several tens of wt. ppm.

Analyses of water in olivine from xenoliths found in kimberlites on the Kaapvaal Craton by Peslier *et al.* (2010) and Baptiste *et al.* (2012) show that the amount of water decreases with increasing pressure (depth), from about 100 wt ppm at 100 km to 10 wt ppm (essentially dry) at 200 km. This was taken by Peslier *et al.* (2010) as explanation for the longevity of cratons. However, very recent work on xenoliths from the Udachnaya kimberlite pipe in Siberia sourced from depths down to 200 km shows high water content in olivine, up to 300 wt ppm, that is depth independent (Doucet *et al.* 2013).

The estimate of water content at 180 km depth beneath the Grenville Province exceeds the values determined by Peslier *et al.* (2010) for the lower lithosphere of the Kapvaal Craton and is therefore consistent with the interpretation of refertilization of parts of the lower Grenville lithosphere. Farther to the northwest on Profile 1, the resistivity decreases to lower values (e.g. as shown by fig. 18 in Adetunji *et al.* 2014), and in the anomaly near the Kirkland Lake and Cobalt kimberlite fields it reaches values of ∼10 Ω m. Explanation of the localized anomaly by the presence of water in the olivine, would require concentrations of several hundred wt ppm, comparable to those noted by Doucet *et al.* (2013).

6.4 Geoelectric strike directions

In this study, a depth-based approach was used for the dimensionality and geoelectric strike analysis. Based on *a priori* information, responses were divided into those corresponding to the upper lithospheric layer (45–150 km) and deeper mantle depths (>200 km). In terms of dimensionality, average GB rms misfit values show that on all four profiles and at all depths the MT responses around the Grenville Front and in the northwestern CGB are compatible with the presence of 2-D resistivity structures. These results justify the application of the 2-D inversion approach for modelling. Farther to the southeast, in the southeastern part of the CGB and the CMB, higher phase tensor skew and GB misfits exceeding 1.5 suggest the presence of more complex 3-D structures, or of lower quality data.

Within the upper lithospheric mantle depth range in areas north of Lake Ontario near the Grenville Front and in the northern CGB, the strike direction is approximately east–west. For Profiles 1 and 2 the azimuth of the conductive direction is N85°E (e.g. Figs 3 and 4).

For Profile 3 the direction is E20°S but examination of GB misfit (Figs 4 and 5) shows that a regional N85°E azimuth is associated with only slightly higher misfit than the E20°S azimuth. The MT data are thus consistent with a common lithospheric strike direction over a ∼300 km (east–west) by 200 km (north–south) region of the northern Grenville Province. This result is in accord with the earlier analysis of Mareschal *et al.* (1995) who determined a regional azimuth of N80°E along Profile 1. However, the tensor decomposition applied in this study shows this azimuth extends significantly farther to the east than interpreted by Mareschal *et al.* (1995); to at least as far as Profile 2.

Comparison of the strike directions (Fig. 3) and 2-D resistivity models (Fig. 9) shows that, on all three profiles, the east-west azimuth (north of the dashed line in Fig. 3) are associated with resistive mantle lithosphere. The observations suggest that the strike direction near the Grenville Front is caused by structures in and near the northwestern margin of the mantle lithospheric resistor. The observed east–west strikes are subparallel to the Archean fabric of the Superior craton and so are consistent with this the resistor being Archean lithosphere. Farther to the southeast, the more erratic strike azimuths and their more common southwest–northeast angle are attributed to the response of Proterozoic Grenville lithosphere.

The depth-based MT tensor analysis provided new results on the strike azimuth at >200 km depth in the Grenville Province in southern Ontario. The results define a regional strike direction of N65°E (±5°) for the whole study area. As noted above, based on the large-scale geoelectric structure, we interpret this depth range to include a significant contribution from the lower lithospheric mantle, so the observed regional strike azimuth may reflect either lower lithospheric or deeper mantle structures.

The strike directions derived in this analysis are compared with the SKS fast direction and the regional Bouguer gravity anomaly map of the study area in Fig. 3. The figure also shows the direction (277°) of the present-day APM defined by Larson *et al.* (1997) based on Global Positioning System (GPS) analyses. The seismic anisotropy information was derived from shear wave splitting measurements by Sénéchal *et al.* (1996), Eaton *et al.* (2004), Rondenay *et al.* (2000), Evans *et al.* (2006) and Frederiksen *et al.* (2006, 2007).

The MT response is compared with the gravity data in order to examine spatial correlation of the MT responses with a measure of the large-scale physical property variation in the upper lithosphere, although it is not expected that the responses are necessarily caused by the same structures. The results show that across the study area there appears to be minimal correlation between spatial variations in the most conductive direction and in the Bouguer anomaly. The spatially confined zone of E20°S strikes southwest of the Grenville Front on Profile 3 for the upper lithospheric mantle lies within the gravity high. However, beyond this observation few trends are evident.

There is significant obliquity between the geoelectric strikes in the lower mantle layer and the SKS fast direction across the northern part of the study area. As noted in the period-based results by Ji *et al.* (1996) and Frederiksen *et al.* (2006), there is a consistent obliquity between the conductive direction at lithospheric depths (N80°E) and the SKS fast direction (N103°E) along Profile 1 in the vicinity of the Grenville Front. The MT results indicate that this relationship persists at least 200 km to the east to Profile 2. The obliquity is explained by the dependence of the MT strike direction on structures in the underlying Archean rocks in the upper lithospheric mantle in contrast to a dependence of the SKS response on deeper sources. Most of the SKS split directions in this region correspond closely to the present-day APM direction (Fig. 3) suggesting an asthenospheric contribution to the SKS response (e.g. Frederiksen *et al.* 2006).

The MT strike directions in the lower mantle layer are also oblique to the APM direction. Based on this obliquity to the present APM we interpret the deeper strike direction to be strongly dependent on the lower lithospheric structure. The strikes are interpreted to be related to deeper features in the resistivity models including the geometry of the base of the resistive blocks on Profiles 2 and 3. The lower lithosphere in the study area is interpreted to have been metasomatized by fluids associated with the Cretaceous kimberlitic magmatism. We therefore hypothesize that the observed deep MT strike azimuth was established at the time of this process and potentially records the plate motion at that time.

7 CONCLUSIONS

The resistivity structure of the lithospheric mantle beneath the Grenville Province in southern Ontario, Canada is investigated using a total of 84 MT sites divided into four profiles. Depth-based MT tensor decomposition methods along with isotropic 2-D inversions are applied. The results from this study enable a much more definitive interpretation of the regional lithospheric resistivity structure than that derived from a single profile in Adetunji *et al.* (2014).

Depth-based dimensionality analysis of the data from all four profiles shows that at lithospheric mantle depths, the MT responses from sites at the Grenville Front and in the northwestern CGB are compatible with the presence of 2-D resistivity structures. This result is further supported by spatial consistency of the geoelectric strike azimuth. Sites in the southeastern part of the CGB and the CMB exhibit more significant 3-D structures. The depth-based analysis of the MT responses also suggests that the lithosphere can be subdivided into upper (45–150 km) and deeper (>200 km) lithospheric mantle layers with dominant regional strike azimuths of N85°E (±5°) and N65°E (±5°), respectively. The result for the upper mantle lithosphere agrees well with the lithospheric strike azimuth of N80°E defined for Grenville Front region in the earlier studies, and provides a larger scale geoelectric strike azimuth that can be used for 2-D modelling of the Grenville Province across the study area.

Isotropic 2-D resistivity models of the study were obtained by inversion of distortion-free MT responses from each profile. The resistivity models of the area include a lithospheric conductor that extends from about 100 to 150 km depth beneath the CMB on Profile 4. The conductor is along strike with a similar one imaged by Adetunji *et al.* (2014) on Profile 1. The observation suggests that very conductive lithosphere exists extensively beneath the CMB in the Grenville Province. The depth of this conductor suggests that the enhanced conductivity may be due to grain boundary graphite films. The source of the graphite is interpreted to have been either fluids associated with the passage of the Cretaceous Great Meteor hotspot or carbon introduced during the pre-Grenvillian tectonism. The mobilization and final emplacement of the graphite could have been during Grenvillian orogenesis or during the Cretaceous kimberlitic magmatic process.

The results from this study show that the entire Grenville Province in southern Ontario is characterized by large-scale, laterally extensive, resistive lithosphere. It extends 300 km southeast beneath the Grenville Province from the Grenville Front to a point about 100 km southeast of the CMBBZ and based on the results for the four profiles, it extends for at least 800 km along-strike. The resistor is interpreted to form part of the Superior lithosphere, the Archean

lithospheric root which provided the stable, cold and low density basement for the Grenville orogen, which supports the earlier interpretation by Ludden & Hynes (2000). Based on the resistivity models, the observed N85°E strike angle in the upper lithospheric layer is interpreted to correspond to the Archean geoelectric fabric of the Superior craton.

The top of the resistor dips to the southeast on Profile 1 and has an overall southeast-dipping trend on Profiles 2 and 3 suggesting overthrusting by Proterozoic Grenville lithosphere. The results of this study show that the base of the lithospheric resistor has significant relief, a result that was not available from the analysis of only Profile 1 in Adetunji *et al.* (2014). The base extends to a maximum depth of ∼280 km on Profiles 2 and 3 and it extends to only ∼150 km on Profiles 1 and 4. It is suggested that the narrow zone of conductive mantle that separates the lithospheric resistors on Profile 4 in southwest Ontario is connected to the more conductive mantle that separates two parts of lithospheric resistor on Profile 3 north of Lake Superior and to the conductive lower lithosphere on adjacent Profile 1. We interpret the observed 280 km depth to be the base on the lithosphere in the region, and the relief on the lower surface of the resistor to be caused by enhanced conductivity in the lower lithosphere. These results revise the earlier interpretation based on only Profile 1 in Adetunji *et al.* (2014).

The enhanced conductivity in the lower lithosphere exhibits high spatial correlation with decreased shear wave velocity. On Profile 1 the enhanced conductivity is bounded to the northwest by a subvertical resistivity anomaly located near the Kirkland Lake and Cobalt kimberlite fields. The connected region of the conductive mantle along Profiles 1, 3 and 4 is therefore interpreted as a zone that has been metasomatized by fluids associated with Cretaceous kimberlite magmatism. The absence of any surface gravity anomalies or surface topography mirroring the spatial variations in the base of the lithospheric resistor suggest that the refertilization has produced minimal changes to the density and thermal properties of the lower lithosphere. The enhanced conductivity is therefore interpreted to be associated with the presence of water in nominally anhydrous minerals. Based on the observed resistivity values of 180 Ω m at 180 km depth, and estimates of the temperature at this depth of 1220 °C, the relationship between resistivity and water content of Jones *et al.* (2012) indicates a water content of approximately 50 wt ppm. Higher water content is required to explain the localized resistivity anomaly observed at 180 km depth in the area of the Kirkland Lake and Cobalt kimberlite fields.

ACKNOWLEDGEMENTS

The authors thank the POLARIS southern Ontario MT team (J. Wenham, M. Serzu, X. Ma, E. Gowan, H. Sealey, T. Pacha, B. Eade, J. McCutcheon, I. Asudeh, C. Andrews, C. Samson and P. Fernberg) for MT data collection and landowners in the region for site access. Comments from A. Frederiksen, A Camacho, the Editor Ute Weckmann, Greg Nieuwenhuis and several anonymous reviewers led to significant improvement of the manuscript. Some figures were produced using Wessel and Smith's GMT package. Funding for POLARIS has been provided by industry, the Canada Foundation for Innovation, provincial agencies from Ontario and British Columbia, the Federal Economic Development Initiative for Northern Ontario, Natural Resources Canada and NSERC (Natural Sciences and Engineering Research Council of Canada). This research was supported by an NSERC Discovery Grant (105748) to Ian Ferguson.

REFERENCES

Abt, D.L., Fischer, K.M., French, S.W., Ford, H.A., Huaiyu, Y. & Romanowicz, B., 2010. North American lithospheric discontinuity structure imaged by Ps and Sp receiver functions, *J. geophys. Res.,* **115,** B09301, doi:10.1029/2009JB006914.

Adetunji, A.Q., 2014. Resistivity structure of the Precambrian Grenville Province, Canada, *PhD thesis,* University of Manitoba, Winnipeg.

Adetunji, A.Q., Ferguson, I.J. & Jones, A.G., 2014. Crustal and lithospheric scale structures of the Precambrian Superior-Grenville margin, *Tectonophysics,* **614,** 146–169.

Adetunji, A.Q., Ferguson, I.J. & Jones, A.G., 2015. Re-examination of magnetotelluric responses and electrical anisotropy of the lithospheric mantle in the Grenville Province, Canada, *J. geophys. Res.*, **120,** doi:10.1002/2014JB011713.

Artemieva, I.M., 2006. Global 1° × 1° thermal model TC1 for the continental lithosphere: implications for lithosphere secular evolution, *Tectonophysics,* **416,** 245–277.

Baptiste, V., Tommasi, A. & Demouchy, S., 2012. Deformation and hydration of the lithospheric mantle beneath the Kaapvaal craton, South Africa, *Lithos,* **149,** 31–50.

Boerner, D.E., Kurtz, R.D. & Craven, J.A., 2000. A summary of electromagnetic studies on the Abitibi-Grenville transect, *Can. J. Earth Sciences,* **37,** 427–437.

Caldwell, T.G., Bibby, H.M. & Brown, C., 2004. The magnetotelluric phase tensor, *Geophys. J. Int.,* **158,** 457–469.

Carr, S.D., Easton, R.M., Jamieson, R.A. & Culshaw, N.G., 2000. Geologic transect across the Grenville orogen of Ontario and New York, *Can. J. Earth Sci.,* **37,** 193–216.

Chave, A.D. & Jones, A.G., 2012. *The Magnetotelluric Method—Theory and Practice*. Cambridge Univ. Press, 570 pp.

Chen, C.-W. & Li, A., 2012. Shear wave structure in the Grenville Province beneath the lower Great Lakes region from Rayleigh wave tomography, *J. geophys. Res.,* **117,** B01303, doi:10.1029/2011JB008536.

Constable, S.C., 2006. SEO3: a new model of olivine electrical conductivity, *Geophys. J. Int.,* **166,** 435–437.

Crough, S.T., 1981. Mesozoic hot spot epeirogeny in eastern North America, *Geology,* **9,** 2–6.

Davidson, A., 1991. *Metamorphism and Tectonic Setting of Gabbroic and Related Rocks in the Central Gneiss Belt,* Grenville Province, Ontario, GAC-MAC-SEG, Toronto, Guidebook, Field Trip A2.

Davidson, A., 1998. Questions of correlation across the Grenville Front east of Sudbury, Ontario, in *Current Research 1998-C,* pp. 145–154, Geological Survey of Canada, Paper 98-IC.

Davis, W.J., Jones, A.G., Bleeker, W. & Grutter, H., 2003. Lithosphere development in the Slave craton: a linked crustal and mantle perspective, *Lithos,* **71,** 575–589.

Doucet, L.S., Peslier, A.H., Ionov, D.A., Brandon, A.D., Golovin, A.V. & Ashchepkov, I.V., 2013. High water contents in the Siberian cratonic mantle: an FTIR study of Udachnaya peridotite xenoliths, in *Proceedings of the Fall AGU,* San Francisco, CA, USA.

Ducea, M.N. & Park, S.K., 2000. Enhanced mantle conductivity from sulfide minerals, southern Sierra Nevada, California, *Geophys. Res. Lett.,* **27,** 2405–2408.

Easton, R.M., 1992. The Grenville Province and the Proterozoic history of Central and Southern Ontario, in *Geology of Ontario, Ontario Geological Survey,* Special Vol. 4, pp. 713–904.

Eaton, D., Frederiksen, A.W. & Miong, S.K., 2004. Shear-wave splitting observations in the lower Great Lakes region: evidence for regional anisotropic domains and keel-modified asthenospheric flow, *Geophys. Res. Lett.,* **31,** L07610, doi:10.1029/2004GL019438.

Eaton, D.W. *et al.*, 2005. Geophysical arrays to investigate lithosphere and earthquake hazards in Canada, *EOS, Trans. Am. geophys. Un.,* **86,** 169–173.

Evans, M.S., Kendall, J.-M. & Willemann, R.J., 2006. Automated SKS splitting and upper-mantle anisotropy beneath Canadian seismic stations, *Geophys. J. Int.,* **165,** 931–942

Faure, S., Godey, S., Fallara, F. & Trepanier, S., 2011. Seismic architecture of the Archean North American mantle and its relationship to diamondiferous Kimberlite fields, *Econ. Geol.,* **106,** 223–240.

Ferguson, I.J., Jones, A.G. & Chave, A.D., 2012. Case histories and geological applications, in *The Magnetotelluric Method: Theory and Practice,* pp. 480–544, eds Chave, A.D. & Jones, A.G., Cambridge Univ. Press.

Forsyth, D.A., Milkereit, B., Davidson, A. & Hanmer, S., 1994. Seismic images of a tectonicsubdivision of the Grenville Orogen beneath lakes Ontario and Erie, *Can. J. Earth Sci*., **31,** 229–242.

Frederiksen, A.W., Ferguson, I.J., Eaton, D., Miong, S.K. & Gowan, E., 2006. Mantle fabric at multiple scales across an Archean-Proterozoic boundary, Grenville Front, Canada, *Phys. Earth planet. Int.,* **158,** 240–263.

Frederiksen, A.W., Miong, S.-K., Darbyshire, F.A., Eaton, D.W., Rondenay, S. & Sol, S., 2007. Lithospheric variations across the Superior Province, Ontario, Canada: Evidence from tomography and shear-wave splitting, *J. geophys. Res.,* **112,** doi:10.1029/2006JB004861.

Griffin, W.L., O'Reilly, S.Y., Doyle, B.J., Pearson, N.J., Coopersmith, H., Kivi, K., Malkovets, V. & Pokhilenko, N., 2004. Lithosphere mapping beneath the North American plate, *Lithos,* **77,** 873–922.

Groom, R.W. & Bailey, R.C., 1989. Decomposition of magnetotelluric impedance tensors in the presence of local three-dimensional galvanic distortion, *J. geophys. Res.,* **94,** 1913–1925.

Groom, R.W. & Bailey, R.C., 1991. Analytic investigations of the effects of near-surface three-dimensional glavanic scatterers on MT tensor decompositions, *Geophysics,* **56,** 496–518.

Hamilton, M.P., Jones, A.G., Evans, R.L., Evans, S., Fourie, C.J.S., Garcia, X., Mountford, A., Spratt, J.E. & the SAMTEX Team, 2006. Electrical anisotropy of South African lithosphere compared with seismic anisotropy from shear-wave splitting analysis, *Phys. Earth planet. Int.,* **158,** 226–239.

Hanmer, S., 1988. Ductile thrusting at mid-crustal level, southwestern Grenville Province, Canada, *Can. J. Earth Sci.,* **25,** 1049–1059.

Hansen, P.C., 1992. Analysis of discrete ill-posed problems by means of the L-curve, *SIAM Rev.,* **34,** 561–580.

Heinson, G., Direen, N.G. & Gill, R., 2006. Magnetotelluric evidence for a deep-crustal mineralising system beneath the giant Olympic Dam iron-oxide copper gold deposit, southern Australia, *Geology,* **34,** 573–576.

Hirth, G., Evans, R.L. & Chave, A.D., 2000. Comparison of continental and oceanic mantle electrical conductivity: is the Archean lithosphere dry?, *Geochem. Geophys. Geosyst.,* **1,** 1030, doi:10.1029/2000GC000048.

Hoffman, P.F., 1989. Precambrian geology and tectonic history of North America, in *The Geology of North America—An Overview,* Vol. A, pp. 447–512, eds Bally, A.W. & Palmer, A.R., The Geological Society of America.

Hunter, R.H. & McKenzie, D., 1989. The equilibrium geometry of carbonate melts in rocks of mantle composition, *Earth planet. Sci. Lett.,* **92,** 347–356.

Ji, S., Rondenay, S., Mareschal, M. & Senechal, G., 1996. Obliquity between seismic and electrical anisotropies as a potentiai indicator of movement sense for ductile shear zones in the upper mantle, *Geology,* **24,** 1033–1036.

Jones, A.G., 1983. The problem of current channelling: a critical review, *Surv. Geophys.,* **6,** 79–122.

Jones, A.G., 1988. Static shift of magnetotelluric data and its removal in a sedimentary basin environment, *Geophysics,* **53,** 967–978.

Jones, A.G., 1999. Imaging the continental upper mantle using electromagnetic methods, *Lithos,* **48,** 57–80.

Jones, A.G., 2012. Distortion of magnetotelluric data: its identification and removal, in *The Magnetotelluric Method: Theory and Practice,* pp. 219–295, eds Chave, A.D. & Jones, A.G., Cambridge Univ. Press.

Jones, A.G., Fullea, J., Evans, R.L. & Muller, M.R., 2012. Water in cratonic lithosphere: calibrating laboratory-determined models of electrical conductivity of mantle minerals using geophysical and petrological observations, *Geochem. Geophys. Geosyst.,* **13,** Q06010, doi:10.1029/2012gc004055.

Jones, A.G. & Groom, R.W., 1993. Strike angle determination from the magnetotelluric impedance tensor in the presence of noise and local distortion — rotate at your peril, *Geophys. J. Int.,* **113,** 524–534.

Jones, A.G., Ledo, J. & Ferguson, I.J., 2005. Electromagnetic images of the Trans-Hudson orogen: the North American Central Plains (NACP) anomaly revealed, *Can. J. Earth Sci.,* **42,** 457–478.

Jones, A.G., Ledo, J., Ferguson, I.J., Craven, J.A., Unsworth, M.J., Chouteau, M. & Spratt, J.E., 2014. The electrical resistivity of Canada's lithosphere and correlation with other parameters: contributions from LITHOPROBE and other programmes, *Can. J. Earth Sci.,* **51,** 573–617.

Karato, S., 1990. The role of hydrogen in the electrical conductivity of the upper mantle, *Nature,* **347,** 272–273.

Kellett, R.L., Barnes, A.E. & Rive, M., 1994. The deep structure of the Grenville Front: a new perspective from western Quebec, *Can. J. Earth Sci.,* **31,** 282–292.

Kellett, R.L., Mareschal, M. & Kurtz, R.D., 1992. A model of lower crustal electrical anisotropy for the Pontiac Subprovince of the Canadian Shield, *Geophys. J. Int.,* **111,** 141–150.

Kennedy, C.S. & Kennedy, G.C., 1976. Equilibrium boundary between graphite and diamond, *J. geophys. Res.,* **81,** 2467–2470.

Korja, T., 2007. How is the European lithosphere imaged by magnetotellurics?, *Surv. Geophys.,* **28,** 239–272.

Korja, T. & Hjelt, S.-E., 1993. Electromagnetic studies in the Fennoscandian Shield—electrical conductivity of Precambrian crust, *Phys. Earth planet. Inter.,* **81,** 107–138.

Kurtz, R.D., Niblett, E.R., Craven, J.A., Stevens, R.A. & Macnae, J.C., 1988. Electromagnetic studies over the Kapuskasing Structural Zone, in *Lithoprobe Kapuskasing Transect,* pp. 167–176, ed. West, G.F., University of British Columbia.

Larson, K.M., Freymueller, J.T. & Philipsen, S., 1997. Global plate velocities from the Global Positioning System, *J. geophys. Res.,* **102,** 9961–9981.

Ledo, J., 2005. 2-D versus 3-D magnetotelluric data interpretation, *Surv. Geophys.,* **26,** 511–543.

Ledo, J., Queralt, P., Martí, A. & Jones, A.G., 2002. Two-dimensional interpretation of three-dimensional magnetotelluric data: an example of limitations and resolution, *Geophys. J. Int.,* **150,** 127–139.

Ludden, J. & Hynes, A., 2000. The Lithoprobe Abitibi-Grenville transect: two billion years of crust formation and recycling in the Precambrian Shield of Canada, *Can. J. Earth Sci.,* **37,** 459–476.

Mackie, R., Rieven, S. & Rodi, W., 1997. User's Manual and Software Documentation for Two-Dimensional Inversion of Magnetotelluric Data, GSY-USA, San Francisco, 14 pp.

Mareschal, J.C., Jaupart, C., Gariepy, C., Cheng, L.Z., Guillou-Frottier, L., Bienfait, G. & Lapointe, R., 2000. Heat flow and deep thermal structure near the southeast edge of the Canadian Shield, *Can. J. Earth Sci.,* **37,** 399–414.

Mareschal, M., Kurtz, R.D., Chouteau, M. & Chakridi, R., 1991. A magnetotelluric survey on Manitoulin Island and Bruce Peninsula along GLIMPCE seismic line J: black shales mask the Grenville Front, *Geophys. J. Int.,* **105,** 173–183.

Mareschal, M., Kellett, R.L., Kurtz, R.D., Ludden, J.N., Ji, S. & Bailey, R.C., 1995. Archean cratonic roots mantle shear zones and deep electrical anisotropy, *Nature,* **375,** 134–137.

Matsuno, T. *et al.*, 2010. Upper mantle electrical resistivity structure beneath the central Mariana subduction system, *Geochem. Geophys. Geosyst.,* **11,** Q09003, doi:10.1029/2010GC003101.

McNeice, G.W. & Jones, A.G., 2001. Multisite, multifrequency tensor decomposition of magnetotelluric data, *Geophysics,* **56,** 158–173.

Meyer, H.O.A., Waldman, M.A. & Garwood, B.L., 1994. Mantle xenoliths from kimberlite near Kirkland Lake, Ontario, *Can. Mineral.,* **32,** 295–306.

Mibe, K., Fujii, T. & Yasuda, A., 1998. Connectivity of aqueous fluid in the Earth's upper mantle, *Geophys. Res. Lett.,* **25,** 1233–1236.

Miensopust, M.P., Jones, A.G., Muller, M.R., Garcia, X. & Evans, R.L., 2011. Lithospheric structures and Precambrian terrane boundaries in northeastern Botswana revealed through magnetotelluric profiling as part of the Southern African Magnetotelluric Experiment, *J. geophys. Res.,* **116,** B02401, doi:10.1029/2010JB007740.

Muller, M.R. *et al.*, 2009. Lithospheric structure, evolution and diamond prospectivity of the Rehoboth Terrane and the western Kaapvaal Craton, southern Africa: constraints from broadband magnetotellurics, *Lithos,* **112S,** 93–105.

Ogawa, Y. *et al.*, 1996. Deep electrical conductivity structures of the Appalachian Orogen in the southeastern US, *Geophys. Res. Lett.,* **23,** 1597–1600.

Park, S.K. & Mackie, R.J., 1997. Crustal structure at Nanga Parbat, northern Pakistan, from magnetotelluric soundings, *Geophys. Res. Lett.,* **24,** 2415–2418.

Parker, R.L., 1980. The inverse problem of electromagnetic induction: existance and construction of solutions based on incomplete data, *J. geophys. Res.,* **85,** 4421–4425.

Parker, R.L. & Booker, J.R., 1996. Optimal one-dimensional inversion and bounding of magnetotelluric apparent resistivity and phase measurements, *Phys. Earth planet. Int.,* **98,** 269–282.

Pearson, D., Boyd, F., Haggerty, S., Pasteris, J., Field, S., Nixon, P. & Pokhilenko, N., 1994. The characterisation and origin of graphite in cratonic lithospheric mantle: a petrological carbon isotope and Raman spectroscopic study, *Contrib. Miner. Pet.,* **115,** 449–466.

Peslier, A.H., Woodland, A.B., Bell, D.R. & Lazarov, M., 2010. Olivine water contents in the continental lithosphere and the longevity of cratons, *Nature,* **467,** 78–81.

Pinet, C., Jaupart, C., Mareschal, J-C., Gariépy, C., Bienfait, G. & Lapointe, R., 1991. Heat flow and structure of the lithosphere in the eastern Canadian Shield, *J. geophys. Res.,* **96,** 19 941–19 963.

Poe, B.T., Romano, C., Nestola, F. & Smyth, J.R., 2010. Electrical conductivity anisotropy of dry and hydrous olivine at 8 GPa, *Phys. Earth planet. Int.,* **181,** 103–111.

Pous, J., Ledo, J., Marcuello, A. & Queralt, P., 1997. On the resolution of the Darai Limestones by two-dimensional MT forward modelling, *J. Geomag. Geoelect.,* **49,** 817–825.

Rivers, T., 1997. Lithotectonic elements of the Grenville Province: review and tectonic implications, *Precambrian Res.,* **86,** 117–154.

Rivers, T., van Gool, J.A.M. & Connelly, J.N., 1993. Contrasting tectonic styles in the northern Grenville Province: implications for dynamics of orogenic fronts, *Geology,* **21,** 1127–1130.

Rivers, T., Culshaw, N., Hynes, A., Indares, A., Jamieson, R. & Martignole, J., 2012. The Grenville orogen—a post-lithoprobe perspective, in *Tectonic Styles in Canada: The Lithoprobe Perspective,* pp. 97–236, eds Percival, J.A., Cook, F.A. & Clowes, R.M., Geological Association of Canada, Special paper 49.

Rodi, W.L. & Mackie, R.L., 2001. Nonlinear conjugate gradients algorithm for 2D magnetotelluric inversion, *Geophysics,* **66,** 174–187.

Rodi, W.L. & Mackie, R.L., 2012. The inverse problem, in *The Magnetotelluric Method: Theory and Practice,* pp. 347–414, eds Chave, A.D. & Jones, A.G., Cambridge Univ. Press.

Rondenay, S., Bostock, M.G., Hear, T.M., White, D.J. & Ellis, R.M., 2000. Lithospheric assembly and modification of the SE Canadian Shield: Abitibi-Grenville teleseismic experiment, *J. geophys. Res.,* **105,** 13 735—13 754.

Schäfer, A., Houpt, L., Brasse, H., Hoffmann, N. & EMTESZ Working Group, 2011. The North German conductivity anomaly revisited, *Geophys. J. Int.,* **187,** 85–98.

Schmoldt, J.-P., 2011. Multidimensional isotropic and anisotropic investigation of the Tajo Basin subsurface: a novel anisotropic inversion approach for subsurface cases with oblique geoelectric strike directions, *PhD thesis,* National University of Ireland, Galway.

Schwarz, G., 1990. Electrical conductivity of the Earth's crust and upper mantle, *Surv. Geophys.*, **11**, 133–161.

Selway, K., 2014. On the causes of electrical conductivity anomalies in tectonically stable lithosphere, *Surv. Geophys.,* **57,** 219–257.

Sénéchal, G., Rondenay, S., Mareschal, M., Guilbert, J. & Poupinet, G., 1996. Seismic and electrical anisotropies in the lithosphere across the Grenville Front, Canada, *Geophys. Res. Lett.* **23,** 2255–2258.

Sleep, N.H., 1990. Monteregian hotspot track: a long-lived mantle plume, *J. geophys. Res.,* **95,** 21 983–21 990.

Sleep, N.H., 2009. Stagnant lid convection and carbonate metasomatism of the deep continental lithosphere, *Geochem. Geophys. Geosyst.,* **10,** Q11010, doi:10.1029/2009GC002702.

Spratt, J.E., Jones, A.G., Jackson, V.A., Collins, L. & Avdeeva, A., 2009. Lithospheric geometry of the Wopmay orogen from a Slave craton to Bear Province magnetotelluric transect, *J. geophys. Res.,* **114,** B01101, doi:10.1029/2007JB005326.

Veeraswamy, K.K., Abdul Azeez, K.K., Gupta, A.K., Babu, N. & Harinarayana, T., 2012. Deep geo-electric structure of the Dhawar craton (India) inferred from magnetotelluric studies, in *Proceedings of the Electromagnetic Induction Workshop,* Darwin, poster 1.3-22p.

Vozoff, K., 1991. The magnetotelluric method, in *Electromagnetic Methods in Applied Geophysics,* pp. 641–711, ed. Nabighian, M.N., Society of Exploration Geophysicists.

Wannamaker, P.E., 1999. Affordable magnetotellurics: interpretation in natural environments, in *Three-Dimensional Electromagnetics,* pp. 349–379, eds Oristaglio, M. & Spies, B., Geophysical Development Series v. 7, Society of Exploration Geophysicists.

Wannamaker, P.E., 2005. Anisotropy versus heterogeneity in continental solid earth electromagnetic studies: fundamental response characteristics and implications for physicochemical state, *Surv. Geophys.,* **26,** 733–765.

Wannamaker, P.E. *et al.*, 1996. Magnetotelluric experiment probes deep physical state of Southeastern U.S., *EOS, Trans. Am. geophys. Un.,* **329,** 332–333.

Weidelt, P. & Chave, A.D., 2012. The magnetotelluric response function, in *The Magnetotelluric Method: Theory and Practice,* pp. 122–162, eds Chave, A.D. & Jones, A.G., Cambridge Univ. Press.

Whitmeyer, S.J. & Karlstrom, K.E., 2007. Tectonic model for the Proterozoic growth of North America, *Geosphere,* **3,** 220–259.

Williams, H.R., Stott, G.M., Thurston, P.C., Sutcliffe, R.H., Bennett, G., Easton, R.M. & Armstrong, D.K., 1992. Tectonic evolution of Ontario: summary and synthesis, *Geol. Ont.,* **25,** 1255–1346.

Wynne-Edwards, H.R., 1972. The Grenville Province, in *Variations in tectonic styles in Canada,* pp. 263–334, eds Price, R.A. & Douglas, R.J.W., Geological Association of Canada Special Paper 11.

Yoshino, T., Manthilake, G., Matsuzaki, T. & Katsura, T., 2008. Dry mantle transition zone inferred from the conductivity of wadsleyite and ringwoodite, *Nature,* **451,** 326–329.

Yoshino, T., Matsuzaki, T., Shatskiy, A. & Katsura, T., 2009. The effect of water on the electrical conductivity of olivine aggregates and its implications for the electrical structure of the upper mantle, *Earth planet. Sci. Lett.,* **288,** 291–300.

Yuan, H. & Romanowicz, B., 2010. Lithospheric layering in the North American craton, *Nature,* **466,** 1063–1069.

Yuan, H., Romanowicz, B., Fischer, K.M. & Abt, D., 2011. 3-D shear wave radially and azimuthally anisotropic velocity model of the North American upper mantle, *Geophys. J. Int.,* **184,** 1237–1260.

Zhang, P., Chouteau, M., Mareschal, M., Kurtz, R.D. & Hubert, C., 1995. High frequency magnetotelluric investigation of crustal structure in north-central Abitibi, Quebec, Canada, *Geophy. J. Int.,* **120,** 406–418.